ELSEVIER

Contents lists available at ScienceDirect

Ultrasonics

journal homepage: www.elsevier.com/locate/ultras



Advancing ex-vivo meniscus tissue characterization: sensitivity and accuracy of shear modulus measurements via supersonic shear imaging vs. biomechanical testing

Sayed Shahabodin Hashemi ^{a,b,*}, Jose Luis Martin-Rodriguez ^{a,d,e}, Angel Ruiz Molina ^f, Antonio Manuel Callejas Zafra ^{a,b,c,d}, Guillermo Rus ^{a,b,c,d}

- ^a Ultrasonics Lab (TEP-959), Department of Structural Mechanics, University of Granada, Granada 18071, Spain
- b Department of Structural Mechanics & Hydraulic Engineering, University of Granada, Polytechnic of Fuentenueva, 18071, Granada, Spain
- ^c Excellence Research Unit "Modeling Nature" (MNat), UGR, Granada, Spain
- d Biosanitary Research Institute of Granada (ibs. GRANADA) Biomechanics Group TEC-12, Granada, Spain
- ^e Hospital Universitario Clínico San Cecilio, Granada, Spain
- ^f Hospital Universitario de Poniente, Almeria, Spain

ARTICLE INFO

Keywords: Meniscus Ultrasound elastography Quasi-static method Dynamic method Shear wave elastography Clinical Diagnosis Receiver Operating Characteristic Curves

ABSTRACT

Non-invasive measurement of meniscal mechanical properties is critical for advancing both meniscal pathophysiology research and represents a critical advancement in musculoskeletal diagnostics. This study aimed to evaluate the accuracy and sensitivity of ultrasound-based stiffness measurements using Supersonic Shear Imaging (SSI) compared to low-strain and high-strain tensile testing and to assess the ability of SSI to detect meniscal degeneration. Sixty bovine menisci were analyzed across seven regions, covering including the tibial and femoral layers, as well as the circumferential region, using shear wave elastography (SWE) and tensile testing. To evaluate tissue degeneration, samples underwent mechanical testing both before and after being subjected to five freeze-thaw cycles. Shear stiffness values obtained from SSI were compared against tensilederived parameters, including shear modulus at low strain, linear stiffness, and Young's modulus measured from stress-strain curves up to failure, assuming small-amplitude shear wave propagation. Depth-dependent effects in Region of Interest (ROI) selection were evaluated, and Different SSI transducers were assessed using various receiver tests. Our results demonstrate significant agreement between SSI measurements and mechanical properties: 88 % sensitivity for stiffness and Young's modulus in circumferential samples, and 91 % for shear modulus at 3 % strain in femoral and tibial regions. While intact samples showed strong positive correlations between stiffness measures, degenerated tissue exhibited inverse relationships. Our comprehensive transducer comparison and receiver tests yielded optimized protocols for ROI selection. Crucially, we identify for depthdependent measurement artifacts, proposing the ROI selection guidelines specific to meniscal elastography. This depth-aware acquisition strategy, together with the observed sensitivity of SSI to degeneration (p < 0.001), supports its clinical utility in contexts where conventional ultrasound elastography is limited. Overall, these findings validate SSI as a sensitive technique for biomechanical assessment of the meniscus, with direct translational potential for diagnosing degeneration and monitoring post/pre surgical tissue remodeling.

1. Introduction

The meniscus is an anisotropic and time-dependent material that functions as a shock absorber, resisting tensile, compressive, and shear forces that are generated during routine activities [1,2]. This enables it

to fulfil its vital role in the knee joint. Meniscus injury has become a common problem in knee joint problems. Therefore, accurate evaluation of meniscus structure and function is essential for the diagnosis and treatment of knee joint diseases [3]. Due to the meniscus' limited healing capacity, early and accurate identification of meniscal injuries is

https://doi.org/10.1016/j.ultras.2025.107771

Received 10 March 2025; Received in revised form 13 July 2025; Accepted 19 July 2025 Available online 23 July 2025

0041-624X/© 2025 The Author(s). Published by Elsevier B.V. This is an open access article under the CC BY-NC-ND license (http://creativecommons.org/licenses/by-nc-nd/4.0/).

^{*} Corresponding author at: Department of Structural Mechanics, University of Granada, ETSICCP, Polytechnic of Fuentenueva, 18071, Granada, Spain. E-mail addresses: e.shahabhashemi@go.ugr.es (S.S. Hashemi), ext.joseluismartin@ugr.es (J.L. Martin-Rodriguez), acallejas@go.ugr.es (A.M. Callejas Zafra), grus@ugr.es (G. Rus).

important to prevent and treat degenerative knee osteoarthritis effectively [4,5]. The menisci are firmly attached to the tibial plateau, converting axial compressive loads into circumferential tensile strains (hoop stress) while limiting radial extrusion [6–8].

Ultrasound elastography is an imaging technique used to assess tissue elasticity without the need for invasive procedures or radiation. SSI is one implementation of Shear Wave Elastography (SWE), developed to utilize ultrafast imaging and focused acoustic radiation force to map tissue mechanical properties. In particular, its ability to assess tissue heterogeneity during scanning makes it a useful tool for detecting early biomechanical changes in pathological tissues. Traditional imaging methods, such as MRI, provide structural information but do not evaluate the mechanical characteristics of the meniscus. [9]. Traditional imaging methods, such as MRI, provide structural information but do not evaluate the mechanical characteristics of the meniscus. SWE addresses this limitation by enabling measurement of the shear modulus and quantifying biomechanical properties. Shear wave elastography has been applied in various organs, including the liver, breast [10], tendons [11,12], cartilage [13], ligaments [14], intervertebral discs [15], and Achilles tendons [16] and carotid artery [17], to measure tissue stiffness in the context of injury detection. Previous studies have validated in vivo measurements of meniscal tissue using SWE against histopathology [3], and MRI [18], showing significant reliability and consistency.

Also, the meniscus is composed of distinct layers, with randomly oriented collagen fibers in the superficial layer and large circumferential bundles interconnected by radial fibers in the deep layer, reflecting its anisotropic fiber network. multiple functions of meniscus are promoted by the inhomogeneous structure and composition of the tissue itself. This complex structure makes it challenging to accurately measure different regions and layers due to variations in fiber orientation and the small size of the tissue, [6]. Considering the collagen fiber network, differences have been observed between the deep and superficial layers of the tissue, [19]. It is therefore vital to emphasize the significance of non-destructive measurement of the stiffness of the circumferential region of meniscal tissue. Moreover, factors such as measurement accuracy, appropriate selection of the region of interest (ROI) and choice of probe, as well as potential operator influence in SSI testing, remain unclear for meniscal tissue. On the other hand it is acknowledged that repeated freeze-thaw cycles can have deleterious effects on tendons and soft tissues, which is related to their structural and chemical composition [20]. Freezing, particularly through repeated freeze-thaw cycles, damages meniscal tissue by inducing osteocyte apoptosis and disrupting the collagen network [21]. This process leads to collagen fibril disorganization and reduced fibril diameter, contributing to a reported 20-30 % decrease in the tensile modulus of porcine menisci after three freeze-thaw cycles [21]. In our previous research, the nature of shear wave behavior in thin meniscal tissue was evaluated based on the extraction of shear phase dispersion curves using two elastography methods, as compared to dynamic compression and tensile tests. It was determined that the viscoelastic properties of menisci can be extracted based on the guided wave in meniscal tissue [22], However, to the best of the authors' knowledge, no study has yet compared SSI measurements validity and reliability with biomechanical testing of the meniscus. This study evaluated the accuracy and sensitivity of SSI in measuring stiffness, comparing it to low-strain and high-strain tensile testing, and examined its effectiveness in detecting meniscal degeneration. It was hypothesized that the freeze-thaw cycle would have an adverse effect on allograft integrity, leading to tissue degradation and a decrease in shear stiffness. Shear wave velocity was assumed frequency-independent across the bandwidth of the mechanical excitation, indicating minimal viscous effects, and that the small shear wave amplitude would allow nonlinear effects to be neglected.

While the meniscus is anisotropic, shear wave propagation in the thickness direction is assumed to probe an "effective" isotropic shear modulus, while wave energy leakage or reflections from side boundaries are minimal due to the meniscus's high aspect ratio. It was assumed

Low-strain tensile tests and dynamic shear effect in SWE measurements probe the same intrinsic stiffness, (shear modulus), despite differing loading modes [22].

Also, it was hypothesized that the SWE value of distinct regions of the meniscus would demonstrate correlation and equivalence with biomechanical stiffness and tissue degeneration, and that SWE could be used to predict meniscus tissue degeneration. SSI testing was performed on a significant number of bovine meniscus specimens for six regions of the femoral and tibial layers and the circumferential region. In contrast, to assess the accuracy and sensitivity of the values obtained from the SSI test, the results for the six regions were compared against the very low strain tensile test and, for the circumferential region, against the Young's modulus and stiffness obtained from the tensile test of the specimens to failure. A comprehensive statistical analysis was then performed to evaluate the results. Moreover, measurement evaluation was conducted using various transducers, and the selection of appropriate ROI was performed through the testing of different receivers, ensuring the establishment of a repeatable test method.

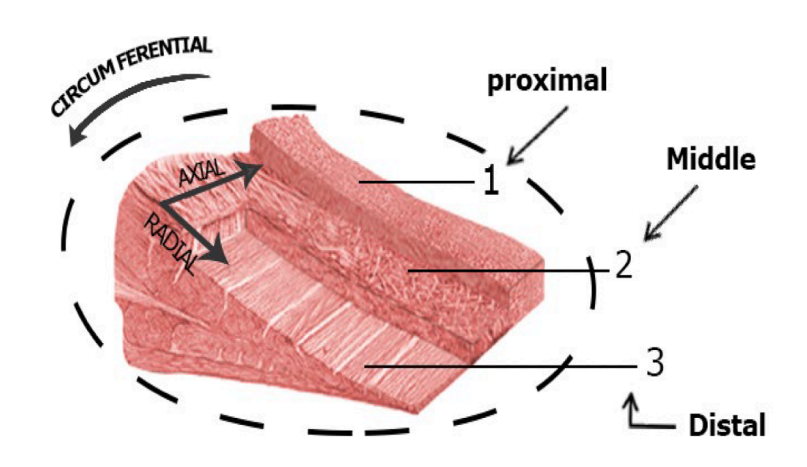
2. Materials and methods

2.1. Study subjects

Sixty fresh bovine menisci were procured from a regulated slaughterhouse and processed under standardized conditions. The specimens were systematically divided into two experimental groups. Group (1) consisted of forty lateral menisci, with twenty serving as fresh controls that underwent immediate mechanical testing within 24 h of acquisition, while twenty matched samples were subjected to five complete freeze-thaw cycles (-20 °C freezing with 37 °C thawing) over a onemonth degeneration period. each sample of this Group (1), after SWE test were carefully sectioned parallel to the superficial layers using a cryotome to maintain anatomical orientation, producing two standardized slices from each meniscus – one from the proximal (femoral) surface and one from the distal (tibial) surface. All sections were maintained in phosphate-buffered saline during preparation to prevent tissue dehydration. Group 2 comprised twenty matched medial-lateral meniscal pairs processed for ultimate tensile strength characterization up to failure. Full-thickness specimens were extracted from the circumferential zone (2.0 \pm 0.3 mm thickness), from which dumbbellshaped samples were cut along the predominant collagen fiber orientation using a biopsy punch. Specimen geometry was verified with digital calipers to ensure compliance with ASTM D638 dimensions (± 10 % tolerance). The tibial and femoral layers were each divided into three sections (Fig. 1). The dumbbell-shaped samples and probe placement were aligned along the axial direction of the tissue fibers.

All specimens failing to meet standardized test parameters, particularly dimensional requirements for the dumbbell-shaped configuration, were excluded. Then samples were subsequently acquired from slaughterhouse sources again to achieve the target of 240 test specimens for both tibial and femoral regions. All specimens underwent standardized SWE assessment immediately preceding tensile testing. To evaluate measurement consistency, we implemented two complementary scanning methodologies. First, two experienced musculoskeletal sonographers, each having performed over 100 clinical meniscus SWE examinations, independently acquired measurements using conventional handheld probe technique. For comparative analysis, we simultaneously employed a mechanical stabilization protocol using an Articulating Arm System with rigid transducer mounting. This setup maintained identical 90° contact angles while eliminating operator-dependent variability.

The 5-cycle protocol has been demonstrated to align with ISO/ASTM standards for tissue biomechanics. This method has been employed to achieve stable degenerated samples. A total of $\underline{20}$ dumbbell-shaped samples were collected from the $\underline{\text{circumferential}}$ area and 240 samples from various regions of the lateral $\underline{\text{distal}}$ and lateral proximal bilayers in





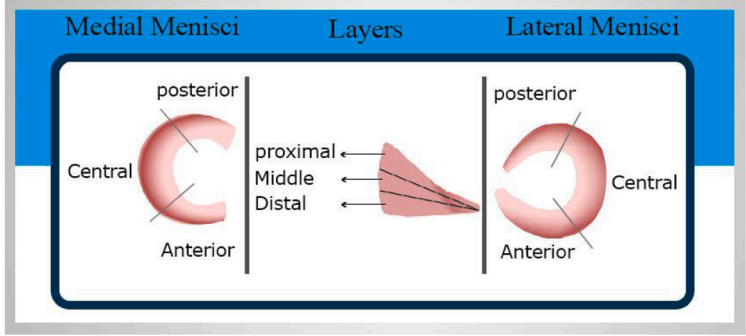


Fig. 1. Schematic of collagen fibers orientation, regions within the meniscus. The schematic in the first picture is a hypothetical figure that has been devised for the purpose of illustrating the fiber orientation that has been selected for this study.

the fresh and degeneration sample groups. The study was conducted in accordance with the ethical guidelines for laboratory samples and the ARRIVE checklist for reporting animal research results.

2.2. Supersonic shear imaging

The SSI device (e.g., Aixplorer, Supersonic Imagine) employs acoustic radiation force to generate shear waves that propagate perpendicularly to the direction of the applied force. By quantifying the shear wave velocity, the system calculates the tissue's shear modulus, enabling quantitative assessment of tissue stiffness. SSI is a specific implementation of Shear Wave Elastography Imaging (SWEI) that utilizes focused beam sequencing to enhance wavefront coherence and improve the signal-to-noise ratio in stiffness estimation, [23]. This method, calculates the initial shear modulus using wave velocity and tissue density based on linear elasticity theory [9]. In fact, shear source moves along the depth at a velocity that is much greater than the velocity of the resulting shear waves.

In the SSI technique, acoustic radiation force focus moves along the depth at a velocity that is much greater than the velocity of the resulting shear waves. This results in interfering shear waves forming a Mach cone, which in turn produces two quasi-plane waves that travel in

different directions. The amplitude of these waves is greater than that of the waves generated in standard SWEI methods, and they travel deeper into the tissue before dissipating, thereby providing a uniform distribution across the studied region. SWEI generates localized shear waves within soft tissue by applying focused acoustic radiation force and measures their propagation speed6 to estimate tissue stiffness.

In the chosen medium, three distinct mechanical waves are generated, namely a fast-propagating compressional wave ($c_T = 1500 \text{ (m/s)}$), a low-frequency shear wave, and a weaker coupling term between the two. It is considered that compressional viscosity is negligible in comparison to shear viscosity. The Voigt viscoelastic framework is utilized to model the low-frequency shear wave, treating it as a propagative diffusion Green's function. This elastic hypothesis is applicable provided that the attenuation length significantly exceeds the wavelength, thereby ensuring that viscosity exerts a negligible influence on shear wave speed and solely affects wave amplitude. It is noteworthy that this assumption is valid for most biological tissues at the frequencies generated by radiation pressure, [9]. However, the Mach angle, which is defined as the ratio between the shear wave speed and the travelling speed of the shear source, is observed to be rather small. In the context of practical medical detection employing the SSI technique, a region of interest is selected, and the mean shear wave speed value is determined.

The strain field resulting from the interaction between the probe and the soft tissue is typically characterized by a lack of homogeneity. However, in instances where the strain gradient within the region of interest is minimal, it is reasonable to hypothesize that the principal stretch ratios in the region are homogeneous, both in the direction of indentation and in the perpendicular directions, [24]. The cross-sectional area of the meniscus was determined by measuring the area of the image of the meniscus that was obtained using the B-mode of the SSI system in conjunction with a linear-array transducer at a frequency of between 4 and 15 MHz and a high frame rate (up to 20,000 frames/s). Following the acquisition of a clear image of the meniscus, the shear wave elastography mode was activated. To circumvent the impact of anisotropy on the measurement process, the probe was meticulously aligned with the direction of the fibers. The image was frozen when the entire ROI was covered by the color and stored for off-line analysis. For the anterior and posterior regions, the shear wave was generated when the image of the crown curvature was clearly visible. The same protocol was repeated for the circumferential region and the associated three regions of the two proximal and distal layers. Each experiment was replicated thrice within each region, and the mean value of these three measurements was calculated for its ROI, which was limited to blue and yellow. The experiment was carried out by two operators (Fig. 2b) and a mechanical arm (Fig. 2a), utilizing two probes and three device modes, with each mode representing a distinct wave generation intensity (see Fig. 2-c and d). Samples were immersed in degassed, deionized water (22 \pm 1° C) during SSI measurements to maintain hydration and ensure acoustic coupling.

2.3. Tensile biomechanical test

The quasi-static tensile test was carried out at a constant ambient temperature of $22\,^{\circ}\text{C}$ with a relative humidity ranging from $85\,\%$ to $90\,\%$. The experiment was conducted using a TA mechanical testing device (Model Number 3200) outfitted with a 450-Newton load cell and the strain was measured from grip to grip. Dumbbell-shaped samples were firmly held between the machine's jaws, which were specifically

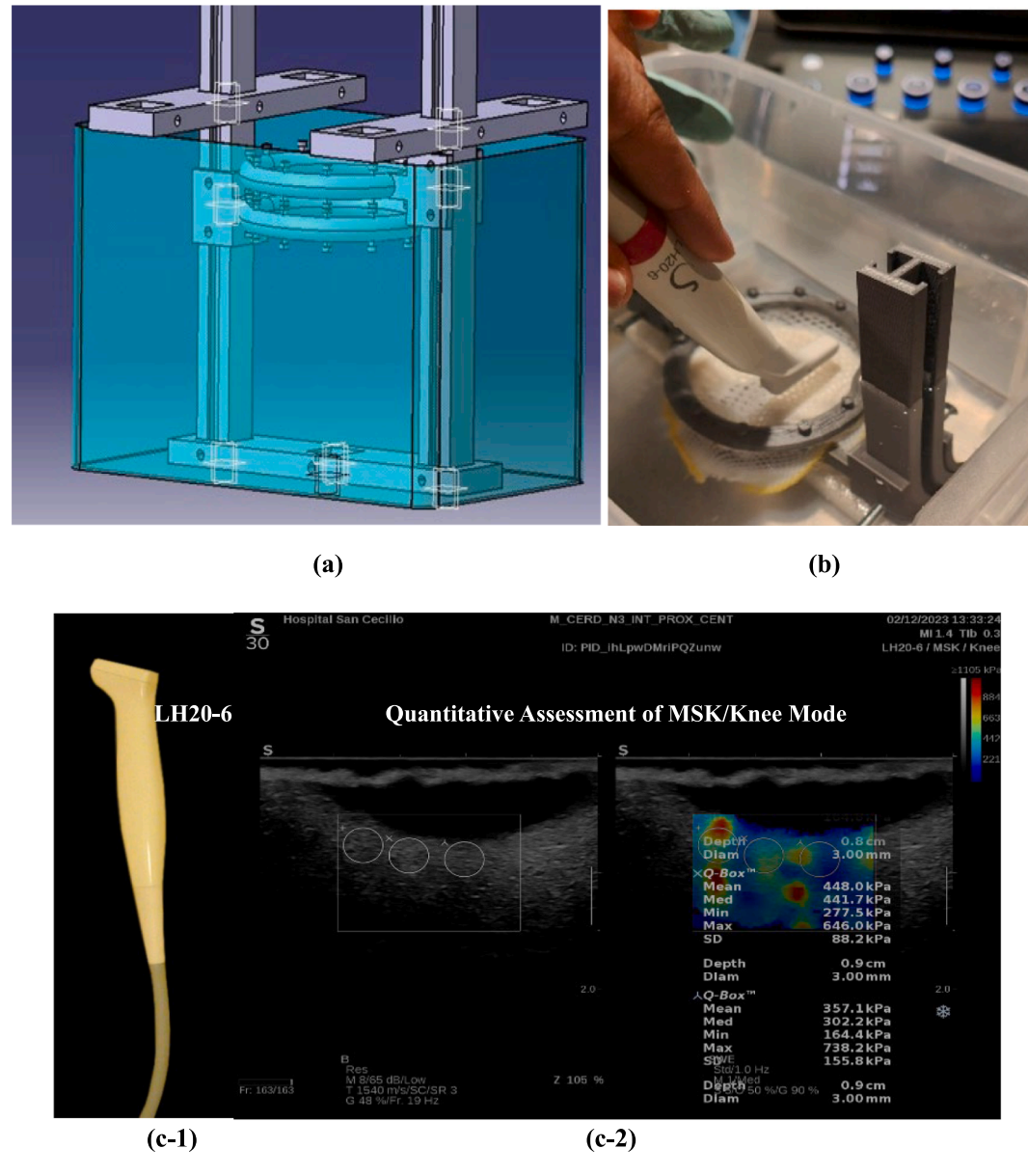
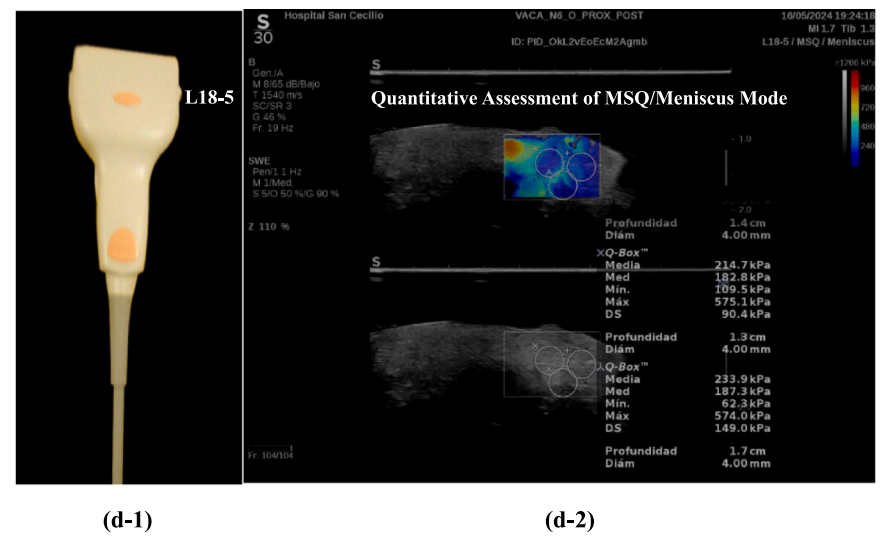


Fig. 2. A: 3D schematic of temperature-controlled water chamber (22 °C) with sample mounting orientation, b: Set-up for Measurements Using SSI by Operators, c-1: LH-20-6 Probe, c-2: Fresh Sample Measurement by LH-20-6 Probe, d-1: L18-5 Probe, d-2: Degenerated Sample Measurement by L18-5 Probe, e: Central Region Measurements, f: Anterior Region Measurement.



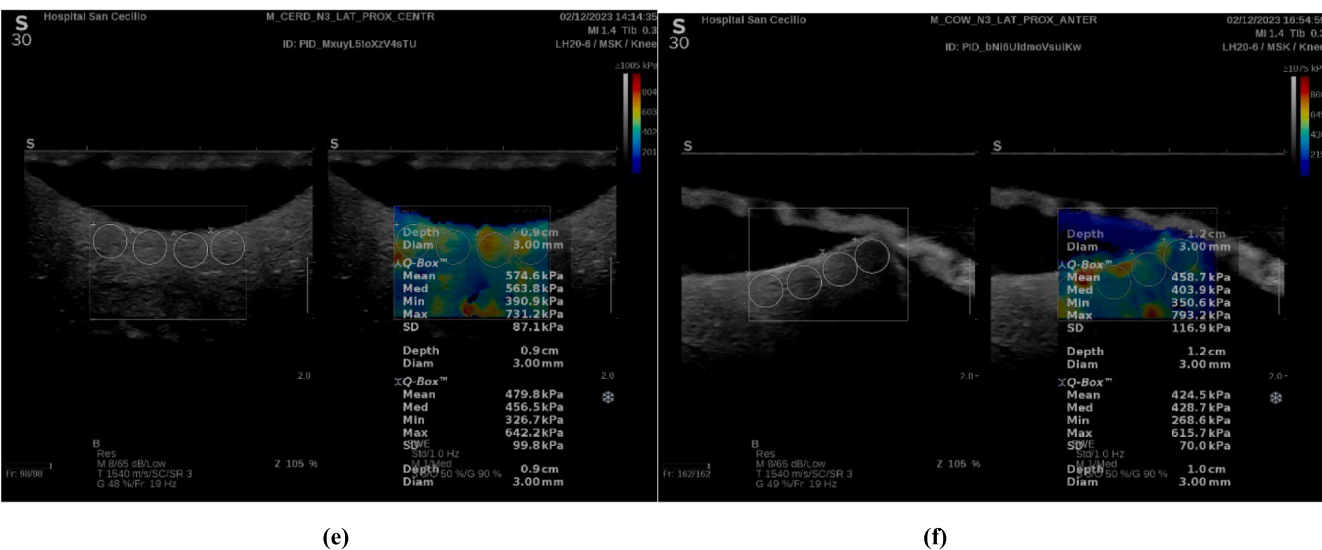


Fig. 2. (continued).

engineered for soft tissue testing (see Fig. 4-a). To ensure proper hydration of the tissue samples, they were sprayed with a phosphate-buffered saline (PBS) solution. Two types of tensile tests were performed on the specimens. In the first group, **low-strain tests** were applied to **longitudinally cut specimens (axial** in circumferential fibers orientation) from the **anterior**, **middle (central)**, **and posterior regions**, covering both the **proximal and distal layers**. In the second group, **high-strain tests to failure** were conducted on **longitudinally cut specimens** from the **circumferential region**, (see Fig. 1).

Group 2 specimens (circumferentially cut samples) underwent tensile testing to failure under standardized conditions: 0.5 mm/s strain rate with a 5 N preload. The strain rate was selected based on three criteria: (1) approximation of physiological loading conditions ($\sim 10~\%$ strain), (2) minimization of interstitial fluid flow artifacts, and (3) consistent measurement of failure properties in tension, [25]. The mechanical test data were collected to calculate the stiffness, ultimate load and Young's modulus for each specimen in group two. The stiffness (k) was calculated from the linear slope of the force-displacement curve following the toe region(see Fig. 3). This experimentally derived stiffness was compared to the theoretical structural stiffness calculated from Eq 1. This validation method served three primary purposes: (i) to directly measure structural stiffness from tensile testing; (ii) to control for the influence of sample dimensions (cross-sectional area A, gauge length L_0) and their potential changes during testing on the resulting

mechanical properties; and (iii) to validate the Young's modulus (E) values predicted by SSI by using them to calculate k. As illustrated in Fig. 3, the schematic of the main mechanical deformations and the representative curves for this study are presented.

$$\begin{cases} E \equiv \frac{\sigma(\varepsilon)}{\varepsilon} = \frac{FL_0}{A\Delta L} \\ Stiffness: k = \frac{EA}{L_0} \end{cases}$$
 (1)

Young's modulus (E) is determined through uniaxial stress testing (either compression or tension), where we measure the material's elastic deformation within the linear portion of the stress–strain curve. The modulus is calculated as the ratio of uniaxial stress (σ) to strain (ϵ), with stress defined as the applied force (F) divided by the cross-sectional area (A) perpendicular to the loading direction ($\sigma=F/A$). Strain represents the relative length change ($\epsilon=\Delta L/L_0$), where ΔL is the deformation magnitude (positive for tension, negative for compression) and L_0 is the original length. These fundamental measurements also enable calculation of axial stiffness (k) for longitudinal structures.

In the Group (1) specimens, specimens were stretched to a strain of 10 % at a rate of 0.00167 1/s and then unloaded. Samples exhibiting slippage were excluded. The stress–strain diagram was analyzed for approved samples within a 3 % strain range (Fig. 4-b). A preload of 1 N was applied to the test specimen to maintain the firmness of the tissue.

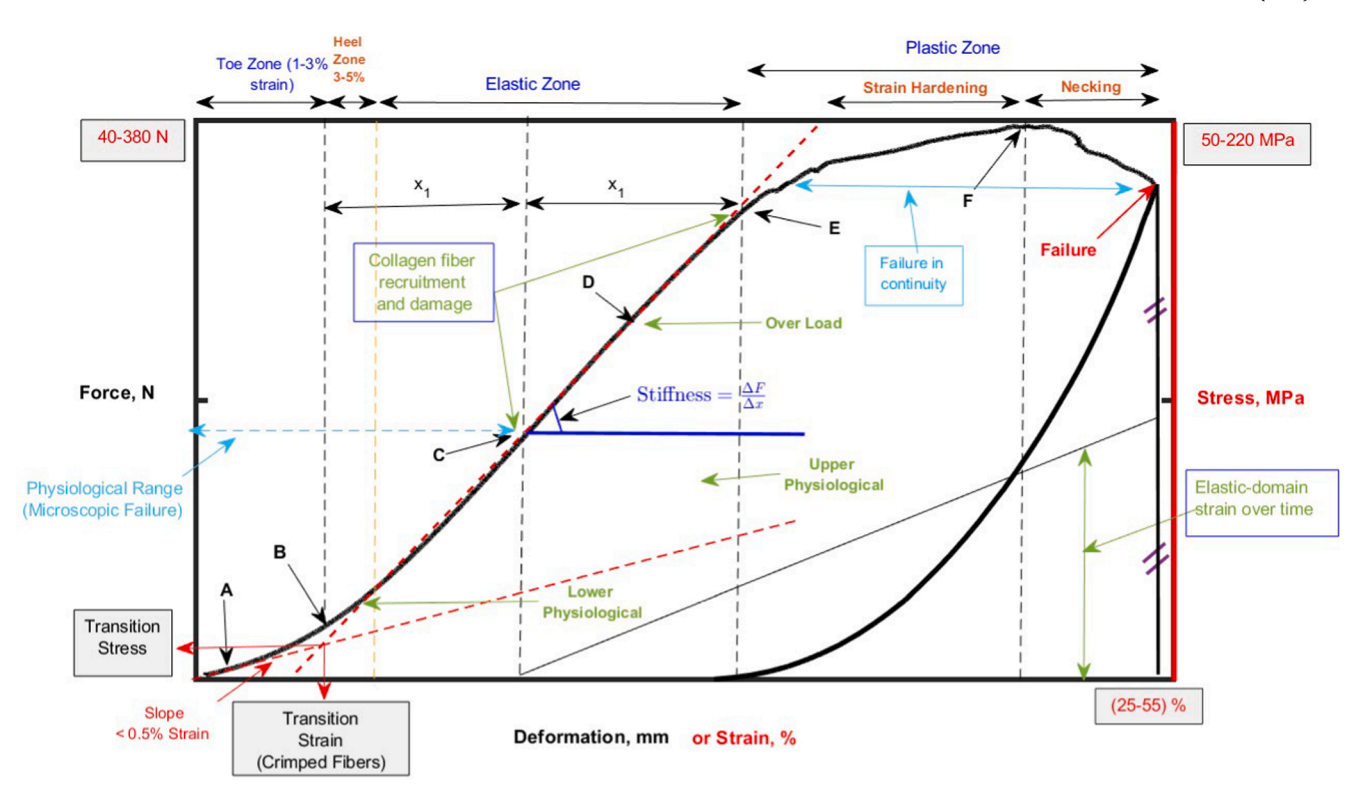


Fig. 3. Schematic of Force-displacement (stress–strain) of bovine meniscus relevant stiffness measured for analysis circumferential region, main mechanical quasi static deformations and representative curves. To describe the material properties, stress (σ) is plotted against strain (ϵ), after normalization according to tissue dimensions. The stress at E represents the yield point, or the onset of failure in continuity. The maximum stress at F represents the ultimate strength. Failure point represents the point at which the tissue loses its continuity and load bearing capacity. The regions A–B and B–E correspond to the toe region and the elastic region of the loading curve, respectively. The area beneath the curve delineated by points A–F is indicative of the tissue's energy to failure and can therefore be interpreted as a measure of the tissue's toughness.

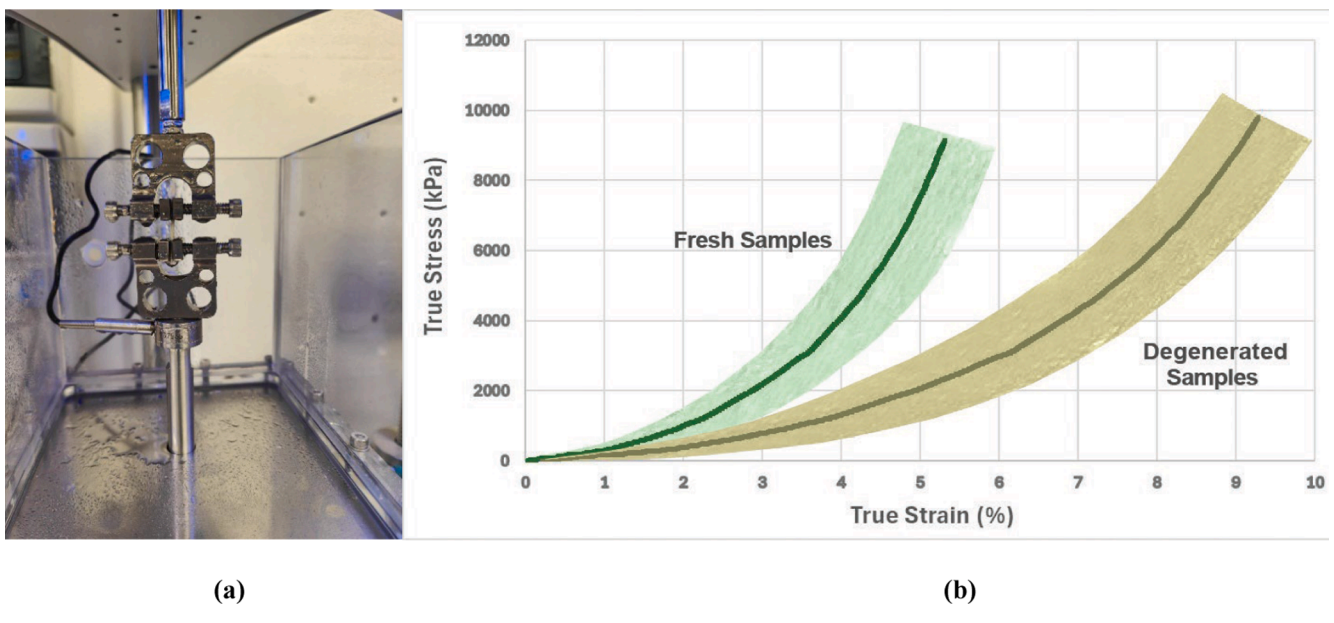


Fig. 4. a: Sample preparation fixed for tensile test, b: comparison of meniscus stress-strain curve in low strain measurements: fresh and degenerated sample.

The calculation of the shear modulus was undertaken based on Hooke's Law, with a Poisson's ratio of 0.45 assumed, aligning with the meniscus's typical range of 0.2–0.6 and supporting the principle of incompressibility [26,27]. Poisson ratio is defined as the ratio of lateral to axial deformation and can be determined through experimental or numerical methods under uniaxial stress, [28]. While it's true that classical

elasticity theory sets $\nu < 0.5$ for isotropic materials (with $\nu = 0.5$ representing perfect incompressibility), biological tissues are often nearly incompressible ($\nu \approx 0.3$ –0.49) due to their high-water content. For both two group, the thickness, length, and width of the dumbbell-shaped specimens were approximately 1.15 \pm 0.12 mm, 24 \pm 2.2 mm, and 7.9 \pm 0.8 mm, respectively. Based on our customized biopsy punch

cutting method, dimensional variability between samples was kept below 10 %. To evaluate the stress–strain curve up to failure, a bimodal power-law model was applied to accurately identify the transition between the linear and nonlinear regions, as described in detail in reference, [29]. Except for the samples in Group (1), due to the large number of specimens and the need to evaluate the ultimate tensile strength of the axial samples from the femoral and tibial layers in comparison to the circumferential region in Group 2, three dumbbell-shaped samples from each of the six regions(n = 18 as subgroup $\mathbf{1}_b$, the results of this group were not included in the analysis with the SWE test) ,were subjected to quasi-static tensile testing until failure.

2.4. Statistical analysis

Data analysis was performed using R-Studio (Posit Software, PBC, Boston, MA, USA). Sample size was determined via regression-based power analysis ($\alpha=0.05$, power =80%, medium effect size ES =0.30). Normality was verified using the Shapiro-Wilk test, and outliers were identified and removed via Grubbs' test. Nonparametric group comparisons were conducted using two-sided Wilcoxon rank-sum tests (significance threshold: *p* <0.05). Correlations between shear wave elastography (SWE) and tensile mechanical parameters were evaluated

using Pearson's *r*, with paired *t*-tests assessing systematic biases. Method agreement was quantified through Bland-Altman analysis. For diagnostic performance, receiver operating characteristic (ROC) curves were generated to compute sensitivity, specificity, and area under the curve (AUC), with optimal thresholds selected by maximizing Youden's index. Additional classification metrics—including accuracy, precision, and F1-score—were derived relative to biomechanical testing as the reference standard. Finally, Tukey's honestly significant difference (HSD) test was applied for multiple pairwise comparisons across meniscal regions.

2.5. Literature review methodology: Tensile mechanical test

To validate the biomechanical measurements obtained in this study, a review of tensile testing methodologies for meniscus tissue was conducted, encompassing peer-reviewed publications from the past three decades. This review served two primary purposes: (1) to establish historical benchmarks for meniscal mechanical properties under both low-strain and failure conditions, and (2) to critically evaluate the methodological heterogeneity in prior studies that may contribute to disparities in reported values. Seven major databases were interrogated—Compendex, EMBASE, MEDLINE, PubMed, ScienceDirect,

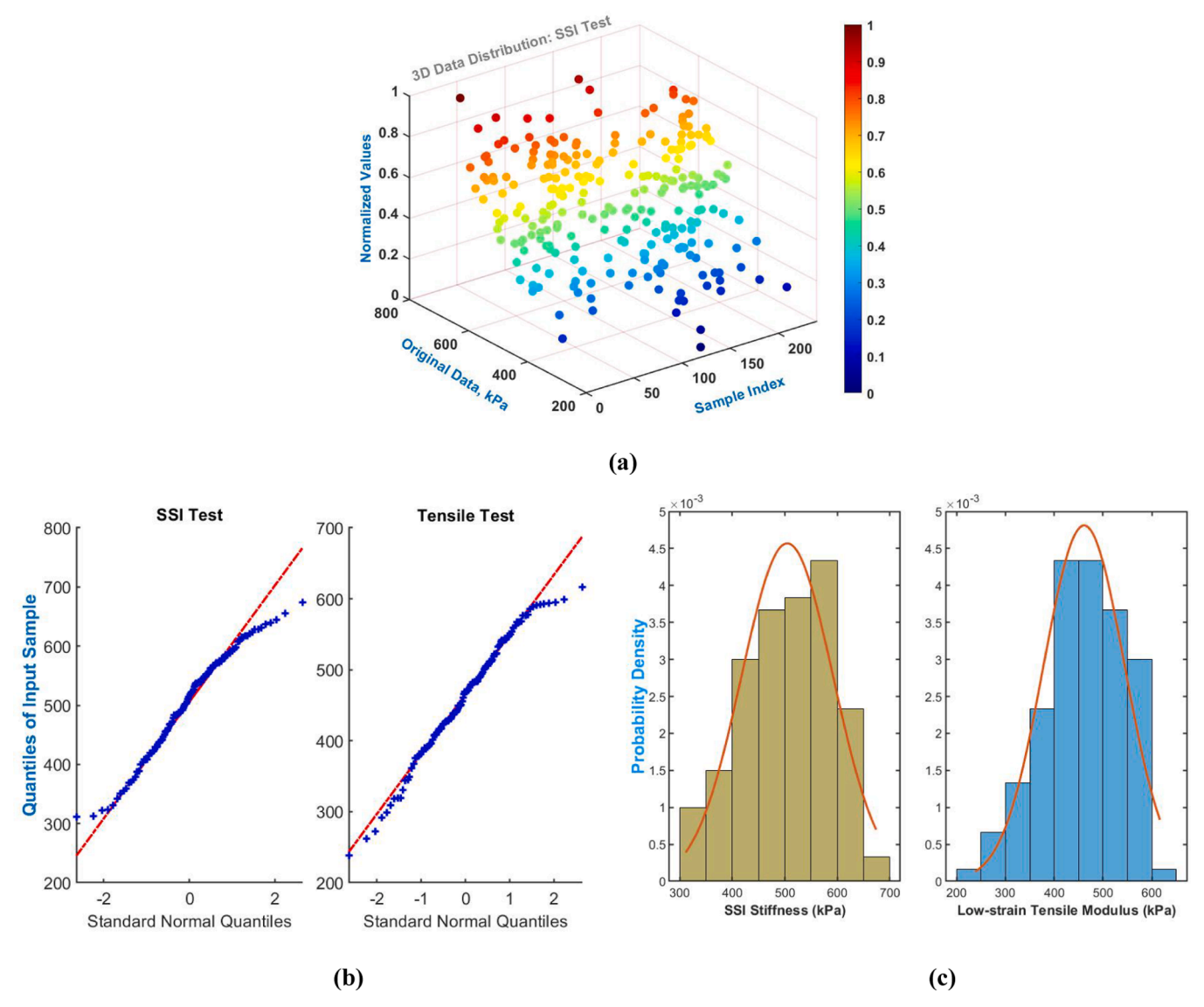


Fig. 5. a: 3D Distribution of SSI measurements for fresh and degenerated menisci, b, c: The Probability density and QQ plots of SSI and tensile tests.

Springer, and Scopus—using targeted Boolean search strings.

Inclusion criteria prioritized studies reporting experimental (non-simulated) tensile data with explicit documentation of testing parameters, including gauge length, strain rate, level of strain and stress, loading direction relative to meniscal fiber orientation, and environmental controls. Particular attention was paid to studies stratifying results by anatomical region (anterior, central, posterior) to account for the tissue's inherent heterogeneity.

3. Results

3.1. Normality evaluation

Initially, the data were assessed for normality using the Shapiro-Wilk test. The results indicated that the null hypothesis of normality could not be rejected (p > 0.05) for the SSI and tensile test mean values, suggesting no significant deviation from a normal distribution. To support this, the data distributions were also visualized using 3D plots, probability density functions (PDFs), and Q-Q plots (see Fig. 5). In the PDF plots, the axis values represent the relative frequency of data occurrences, consistent with standard practices in probability density visualization. Normality of the data was confirmed using Shapiro-Wilk tests as for SSI, W=0.96 and p=0.897, and for tensile test, W=0.93 and p = 0.51, indicating that the data from all two tests were normally distributed. The findings of this study demonstrate that there is no statistically significant deviation from normality observed in either data set. ANOVA results indicated that the between-group variation was minimal compared to the within-group variation, with an F-value = 0.218 and a p-value = 0.398, suggesting that most variability arose within groups rather than between them. Statistical analysis of data from two shear modulus tests (SSI, Tensile test) revealed no statistically significant differences between the groups tested.

3.2. Meniscal tensile test

The tensile test results of this study, in conjunction with a concise synopsis of meniscus tensile experiments documented in the extant literature, are presented in Table 1, arranged in chronological order from 1993 to the present study. Initially, 2472 publications were identified; of these, 20 publications met all eligibility criteria following abstract and full-text screening. The synthesis of these data revealed three critical trends: First, sample sizes in prior work were frequently inadequate (median n < 48, tensile test specimens) to address regional variability, underscoring the statistical advantage of our larger cohort (n = 240). Second, methodological reporting gaps, especially in strain rate and preconditioning protocols,complicated direct comparisons. Third, despite these variances, aggregated low-strain moduli and ultimate strain values fell within defined physiological ranges, supporting the plausibility of our measurements.

These historical data are comprehensively tabulated in Table 1, which juxtaposes key mechanical properties against their original sources while annotating testing conditions. This comparative framework not only contextualizes our results but also highlights the engineering and clinical relevance of standardized reporting—specifically, the need for explicit documentation of gauge lengths and strain rates to enable cross-study *meta*-analyses. By aligning our protocols with the most reproducible methods identified in this review, we ensure that our tensile and supersonic shear imaging (SSI) data provide reliable, translatable benchmarks for future research.

3.3. Validation of SSI for meniscus tissue biomechanics

In the statistical analysis, following the determination of the normality of the data, the correlation and equivalence of the two tests were evaluated using Pearson and Altman standard tests, respectively. As demonstrated in Fig. 6, an acceptable correlation of nearly 80 % is observed between the results for **fresh samples**. However, the values for each region separately show better results. As illustrated in Table 2, in the lowest case, 81 % and in the best case, 93 % correlation was observed for the anterior and posterior regions, respectively. To assess the reliability of two tests, the bias among different methods for all regions were compared by Bland-Altman test. Fig. 7 illustrates the shear stiffness values from SSI (with LH20 probe) for the six regions of the meniscus. Correlation and equivalence studies have shown an agreement between stiffness values obtained from SSI technique, confirming their reliability in evaluating tissue mechanical properties.

In Group 2 specimens, we identified a significant correlation between shear modulus values derived from elastography and both linear stiffness, and Young's modulus measured from stress–strain curves up to failure, obtained from tensile testing. This relationship, illustrated in Fig. 8, demonstrates that supersonic shear imaging accurately captures the full spectrum of meniscal mechanical behavior — from initial linear elasticity to ultimate failure properties.

3.4. SWE diagnostic classification accuracy

The heatmap provides a visual representation of the counts in each category, with darker colors indicating higher counts, thus visually emphasizing the performance of the model in different classifications. To evaluate the overall accuracy and sensitivity of SSI measurements compared to biomechanical testing, the model demonstrated successful detection in seventy-eight (etc. 45 + 33) positive cases and thirty (etc. 8+ 22) negative cases out of 131 successful measurements, missing only fourteen (etc. 8+6) positive and eight (etc. 5+3) negative cases (see Figs. 9 and 10). It is noteworthy that, for each region, the results consistently exhibited diagnostic balance, even in the least favorable scenario. Among the 240 measurements conducted, Figs. 9 and 10 present data from 131 representative experiments demonstrating optimal sensitivity and accuracy, as evidenced by their ROC curves. The remaining measurements (n = 109) exhibited consistent trends with these results. Table 2 shows the results of evaluating the size of the two SSI tests against the biomechanical tensile test for different areas as complete quantitative findings (n = 240).

The confusion matrix heatmap visualizes classification outcomes of the diagnostic model, with misclassifications primarily occurring at tissue boundaries and in degenerated zones. As detailed in Table 2, the proportion of errors appeared in regions where clinical decisions typically rely on combined imaging and history. Despite these edge cases, the model achieved an AUC of 0.89. Region-specific thresholds and revised error maps (Figs. 9 and 10) were incorporated to mitigate false predictions, which remained within acceptable clinical error margins (12.9 % total misclassification rate). On the other hand, although the F1 score and accuracy of SSI classification relative to tensile testing were slightly lower (70-78 %) compared to the mean sensitivity and specificity (>85 %), this disparity may be attributable to the inherent distinctions between the two modalities. Misclassifications typically occurred in borderline or early-degenerative samples, suggesting that SSI may detect viscoelastic changes before structural compromise. The use of Youden's Index ensured optimal thresholding, and ROC analysis

Table 1Summary of meniscus tensile experiments reported in the literature arranged in chronological order from 1993 to present study. C, R, and A stand for circumferential, radial and axial directions. Ant, Cir, Mid, Pos are anterior, circumferential, middle and posterior zones, (for Example: CA is the designation for the circumferential zone, and axial fiber direction. VDA is an acronym that stands for videotape dimension analyzer system. Last update on 2025/07/25.

N	Reference	Year	Species	Region	lateral medial	Number of specimens	Stress at UTS (MPa)	Strain rate	Stated specimen exclusion	Strain Level Used % or mm	Mean of Tensile Moduli (MPa)	Strain measurement
1	Current Study	2025	Bovine	Cir Ant Mid Pos	<u>50</u> + 3	- CA: 40 - A _{1b} :18 - A: 240	$\begin{array}{l} -\text{ CA: } 39.90 \pm 7.84 \\ -\text{ A}_{1b}\text{: } 31.26 \pm 4.25 \\ -\text{ A: Stress controlled (Load/unload)} \end{array}$	CA: 0.00167 s ⁻¹ A: <u>1 mm/</u>	√	CA: Strain toFailureA: 3 %	 CA: 228 ± 53, A1b:191 ± 39, 1.23 ± 0.37 	Grip Displacement
2	1- S.S. Hashemi et al [22].	2025	Porcine	Ant Mid Pos	22 0	AC: 129	Stress controlled (Load/unload)	$\frac{\text{min}}{0.001} \text{ s}^{-1}$	\checkmark	1.5 %	0.6 ± 0.18	Grip Displacement
			Human	Ant Mid Pos	8 8	AC: 48	Stress controlled (Load/unload)	$0.001~{\rm s}^{-1}$	√	1.5 %	0.5 ± 0.22	Grip Displacement
3	Long et al[30].	2024	Porcine	Ant Mid Pos	8 8	A: 27 R: 28	A: 39.30 ± 13.50 R: 10.30 ± 4.25	0.0085 mm/s	\checkmark	Strain to Failure	_	Grip Displacement
4	Morejon et al [31].	2023	Porcine	Mid Cir	10 10	A: 16R: 16	A: 20.30—27.50R: 1.30—2.20	0.01 mm/s	\checkmark	Strain to Failure	A: 132.8 ± 38.1 R: 13.9 ± 9.1	Grip Displacement
5	Gonzalez-Leon et al [19].	2022	Porcine	Ant Mid Pos	8 8	A: 24R: 24	A: 17.70—25.43R: 2.39—4.08	$1 \% s^{-1}$	\checkmark	Strain to Failure	A: 110 ± 60 R: 10 ± 4.8	Grip Displacement
6	Yin et al [32].	2021	Human	Ant Mid Pos	0 7	R&C- N/A: 21	-	1 mm/min	-	Strain to Failure	$\begin{array}{c} 0.171 \pm 77.3 \\ 0.109 \pm 39.9 \\ 0.229 \pm 87.5 \end{array}$	Grip Displacement
7	Nesbitt et al [33].	2021	Human	Ant Pos	6 15	R&C- N/A: 40	A: 5.3 ± 2.7 R: 0.21 ± 0.17	1 % strain/	\checkmark	Strain to Failure	A: 109.9 ± 40.8 R: 1.67 ± 0.67	Grip Displacement
8	D. Warnecke et al [34].	2020	Human	Ant Mid Pos	24 0	A: 66	-	5 %l ₀ /min	\checkmark	Strain to Failure	A: 29 ± 10 (at 5 % of the ascent linear portion)	Grip Displacement
9	Ahmad et al (34).	2017	Human	N/A	12 12	A: 24	_	_	\checkmark	-	99 ± 58	Grip Displacement
10	Barton [35].	2017	Porcine	Mid	5 8	A-N/A: 63	A: 12.12 R: 7.32	5 mm/min	_	Strain to Failure	A: 100–300 R: 10–30	Grip Displacement
11	Peloquin et al. [36].	2016	Bovine	Mid	N/A 10	A-N/A: 95	A: 26.00 ± 12.00 — 36.00 ± 8.00 R: 3.60 ± 1.60 — 4.90 ± 2.70	0.5 mm/s	-	Strain to Failure	A: 215 ± 86 R: 19 ± 10	Grip Displacement
12	Mitchel et al. [37].	2016	Human	Mid	0 N/A	R: 48	_	0.5 mm/s	\checkmark	Strain to Failure	N/A Just Force Calculating	Grip Displacement
13	Yan et al.[38].	2015	Human	Mid	N/A	20A	3–12.38	0.0167 mm/s	_	dynamic tensile preload and then Strain to Failure	3–12	Grip Displacement
14	Lakes et al[39].	2015	Porcine	Mid	0 12	(slices thickness:0.45 mm) - 6A, - 6R	PBS(R): 3.3841 PBS(A): 21.9750 Bsf(R): 3.7500 Bsf(A): 22.8750	1 % strain/ s	√	From 1.3 % strain to rapture	A:118 \pm 48 R:19 \pm 11	Grip Displacement
15	K.M. Fischenich [40]	2015	Human	Ant Pos	12 12	A: 72	-	0.1 mm/s		Strain to Failure	168.8 ± 62.5	Acquired Images
16	Abdelgaied et al [41].	2015	Porcine	Mid	0 15	A: N/A	35.81 ± 9.70	0.00167 s ⁻¹	\checkmark	Strain to Failure	140 ± 32	Grip Displacement
											(con	tinued on next page)

	`											
z	Reference	Year	Species	Region lateral medial	lateral medial	Number of specimens	Stress at UTS (MPa)	Strain rate	Stated specimen exclusion	Strain Level Used % or mm	Mean of Tensile Moduli (MPa)	Strain measurement
17	17 Tanaka et al. [42].	2014	Porcine	Mid	6 0	A: 36	37.80 ± 7.70	10 mm/ min	>	Strain to Failure at: (29.9 \pm 4) %	209.2 ± 35.2	Grip Displacement
			ovine	Mid	0 5	A: 20	36.20 ± 4.70	10 mm/ min	>	Strain to Failure at: (36.0 \pm 1.9) %	186.5 ± 32.4	Grip Displacement
			Human	Mid	0 5	A: 20	11.70 ± 2.10	10 mm/ min	>	: (20.8	97.7 ± 21.8	Grip Displacement
18	Tissakht and Ahmed [43]	1995	Human	Ant Mid Pos	8 18	N/A	A: 11.83—18.83R: 0.81—4.12	$(5\pm1)\ \%$ min^{-1}	>		A: 156 ± 48 R: 12 ± 5	Grip Displacement
19	Skaggs et al. [44].	1994	Bovine	Ant Mid Pos	0 20	RC: 60 (Slices thickness: 0.4 mm)	3.00 ± 2.00	$0.005 \mathrm{s^{-1}}$	ı	Strain to Failure	48 ± 18.6	VDA
20	Anderson et al. [45].	1993	Sheep	Ant	0 10	A: 20	Ant: 22.90 \pm 1.00Pos: 24.50 \pm 0.90	0.5 mm/ min	_	Strain to Failure	$191\pm25\\230\pm34$	VDA

further validated SSI's diagnostic potential despite biomechanical variability. Furthermore, Quantitative analysis revealed no statistically significant difference (p = 0.058) between shear wave elastography measurements obtained by experienced musculoskeletal sonographers and those acquired using the standardized articulated arm fixation system.

4. Discussion

To the best of our knowledge, this is the first study to evaluate ultrasound measurements using supersonic shear imaging (SSI) for assessing meniscus tissue stiffness in comparison to biomechanical testing. Furthermore, our findings demonstrate the capability of real-time elastography to detect damaged meniscal tissue with over 90 % accuracy across six primary femoral and tibial regions, as well as the Circumferential zone. Our findings align with existing literature utilizing biomechanical testing, MRI and histological analysis [3,18,36,34,46–48]. Throughout this research, we clarified the selection process for the region of interest (ROI) and the impact of different transducer choices made by various users.

While previous studies have validated SSI stiffness measurements against histology and MRI, our work provides the first direct accuracy assessment against biomechanical testing. This represents a crucial advancement, as biomechanical validation is essential for establishing SWE as a reliable non-invasive method to identify meniscal pathophysiology. The study assumes a linear elastic behavior for osteoarticular tissue in elastography analyses, a widely accepted approach in both transient elastography and magnetic resonance elastography (MRE) [9,16,20,49,50,51], Due to the low amplitude of shear waves, nonlinear effects are negligible, and viscosity is considered insignificant, as previous research has shown that shear wave velocity remains nearly independent of mechanical shock frequency in SSI. This supports the validity of the measured shear elastic modulus [9].

Correlation studies between SSI-derived shear stiffness and tensile testing confirm considerable consistency across six meniscal regions (femoral and tibial layers). These results reinforce the reliability of elastography in assessing tissue mechanics, supporting its potential for biomechanical research and musculoskeletal diagnostics.

The observations indicate that ultrasound shear wave elastography (SWE) measurements are correlated with tissue stiffness, both for small strains in the tibial and femoral regions and for large strains in the peripheral region. This finding is a notable innovation of this study, as previously significant correlations with tendon and Achilles tendon stiffness had only been observed for small strain elongations in the literature, [47]. The validity of these findings is further supported by the validation of SSI measurements against histopathology by Park et al. [3], and the impressive accuracy of MRI measurements for the meniscus by Ens et al, [18].

It is vital to acknowledge that in pure shear testing, the mechanical behavior is predominantly determined by the solid phase, which consists of proteoglycans and collagen. From a mechanical perspective, collagen fibers in the circumferential region of the tissue are predominantly oriented perpendicular to the shear plane and are stretched during shear loading, contributing to the overall shear stiffness of the tissue. In light of this, it can be argued that this was the strongest rationale for using Young's modulus and stiffness values obtained at the failure point to biomechanically evaluate the circumferential region in comparison to SSI measurements. The results of the correlation and the receiver operating characteristic (ROC) analysis demonstrate a reliable balance between the parameters obtained for the circumferential region and tensile testing to failure.

4.1. Evaluation of meniscal degeneration

It is noteworthy that our innovation holds significant value, particularly in verifying the capability of SSI-derived measurements to

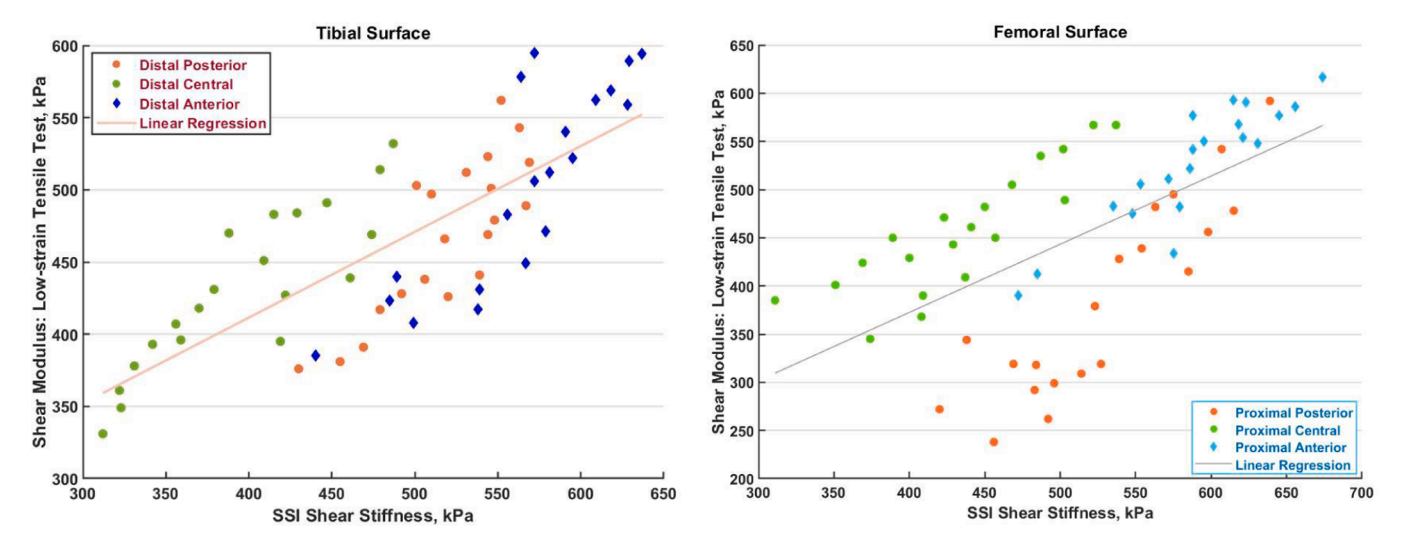


Fig. 6. Fresh samples: Correlation between the estimation of average shear modulus values: experiment SWE test against tensile test, While the figure shows significant differences in values due to the meniscus's inherent regional heterogeneity, the measurements for each region (red, green, and blue) fall within the expected range, confirming equivalence: Probe Placement with ROI Depth 9–15 mm.

 Table 2

 SSI Measurements Versus Tensile Test Analysis.

SSI Test Against Tensile Test	Femoral Surface Probe Placemer ROI Depth 9–15)	Tibial Surface (I Probe Placemen ROI Depth 9–15	Circumferential			
	Anterior	Central	Posterior	Anterior	Central	Posterior	Total	
CTH for SSI (kPa)	575.4	435.6	515.9	555.2	437. 5	529.3	440.25	590.6
Sensitivity%	92.2	85.2	94.7	91.5	79.8	96.3	0.8975	93.4
Specificity%	78.5	84.8	79.2	87.2	97.1	83.4	0.8483	84.4
Accuracy%	81	90	83	78	81	86	0.8633	86.3
Precision%	77	89	81	79	97	77	83	71
F1 Score	78.5	80.6	73.3	78.5	81.6	73.3	79.8	72.2
R^{2} %	91	89	81	90	93	84	0.80	0.79
Limitations	Moderate	Moderate	Moderate	Moderate	Moderate	Moderate	_	Moderate
	specificity	sensitivity	specificity	Accuracy	Sensitivity	Specificity		specificity
Key Strengths	Specificity/	Accuracy/	Specificity/	Specificity/	Sensitivity/	Sensitivity/	Strong	Strong Balance
. 3	Precision	Precision	Precision	Precision	Specificity	Accuracy	Balance	Ü

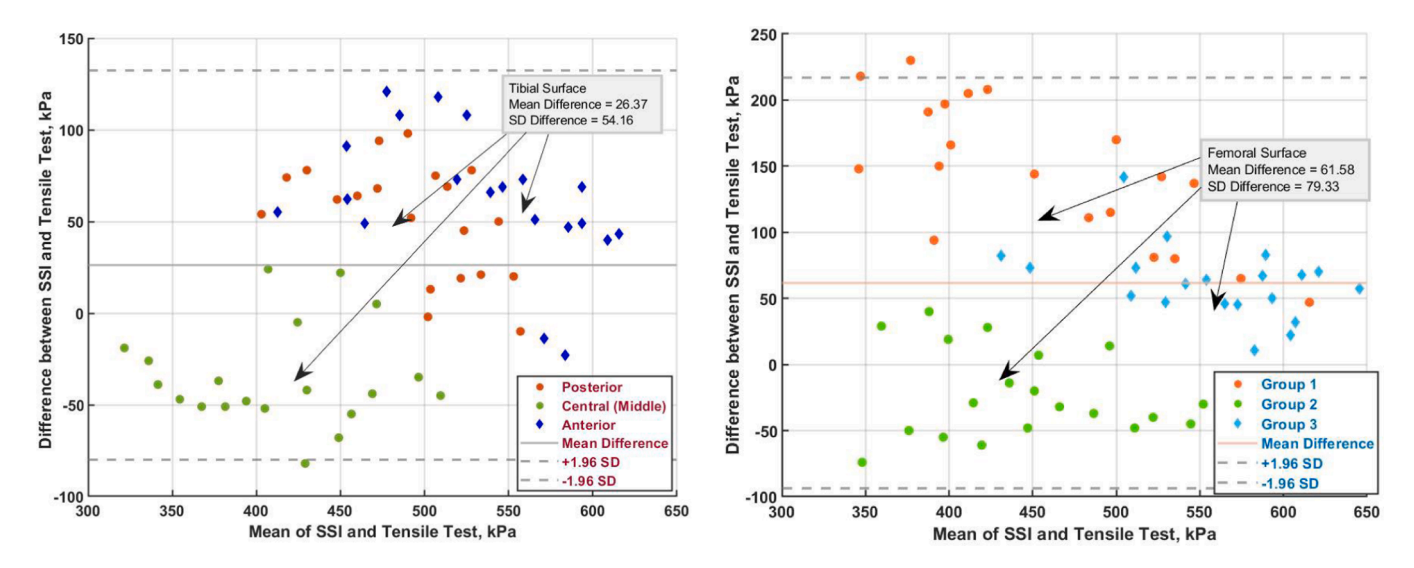


Fig. 7. Fresh samples: Difference between stiffness meniscus by SWE and tensile test: for the three regions of both distal and proximal layer. While the figure shows significant differences in values due to the meniscus's inherent regional heterogeneity, the measurements for each region (red, green, and blue) fall within the expected range, confirming equivalence.

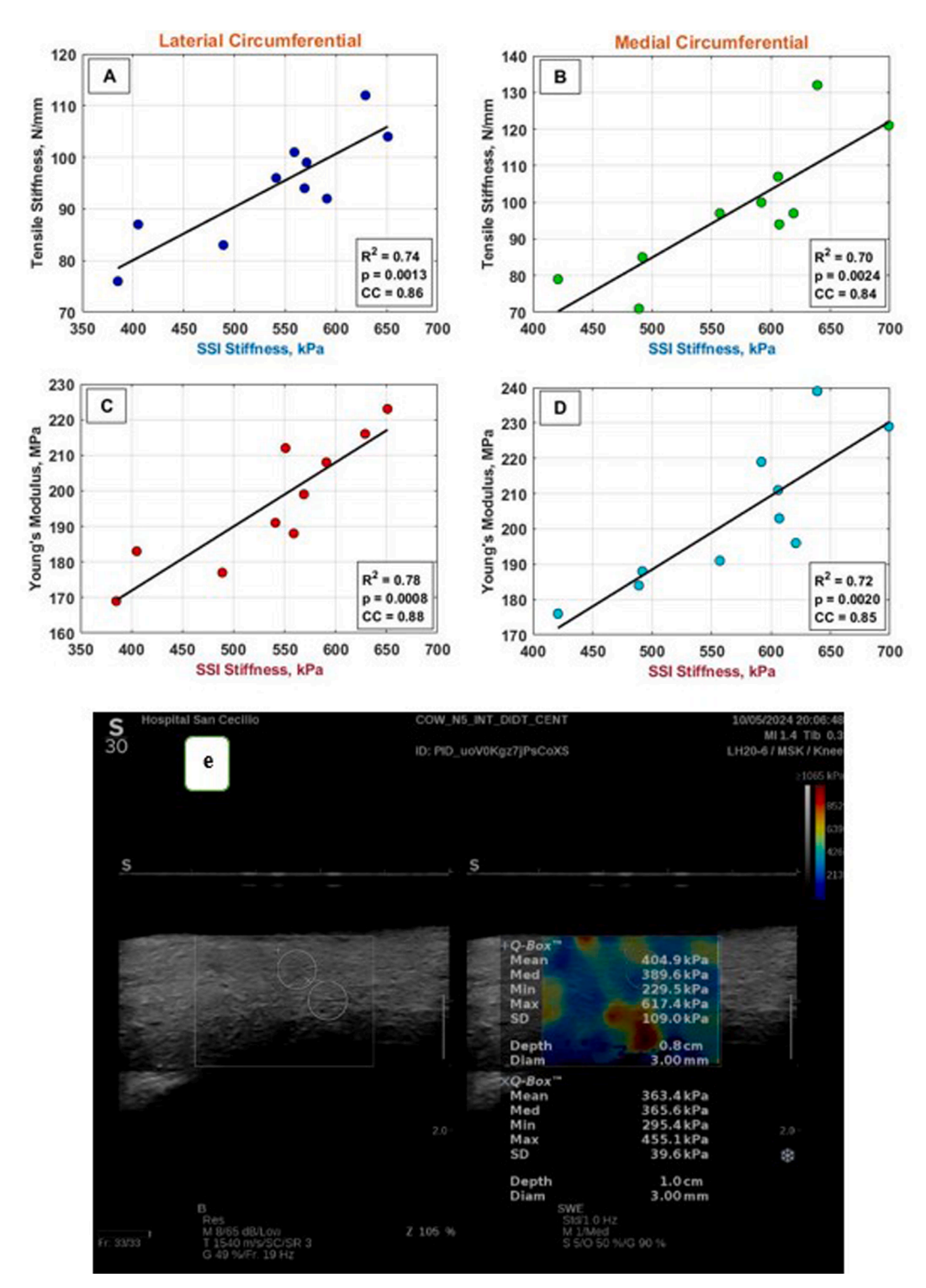


Fig. 8. (a) and (c): SSI vs. tensile stiffness and young's modulus, respectively, for lateral menisci. (b) and (d) SSI vs. tensile stiffness and young's modulus, respectively, for Medial menisci. (e): example of the lowest value of SSI measurements by LH20-6/MSK/knee probe for circumferential region.

effectively detect controlled degenerative meniscus injuries, which could serve as a foundation for further pathological investigations. Furthermore, it is important to emphasize that meniscal degeneration is closely associated with the onset and progression of osteoarthritis. During the degenerative process, collagen and glycosaminoglycan (GAG) content decreases, while the fluid fraction of the tissue increases [39]. This shift impacts the tissue's ability to dissipate energy, alters its load-bearing capacity, and affects its structural alignment.

On the other hand, Previous biomechanical and biochemical studies

have demonstrated that multiple freeze—thaw cycles result in soft tissue allograft damage, despite an increase in water content, [52,53]. As demonstrated in Fig. 11, our findings reveal a substantial discrepancy between the fresh and frozen (degenerated) groups, thereby substantiating our hypothesis.

Stiffness values obtained from real-time elastography testing were lower across all regions in degenerated samples compared to fresh samples. Similarly, shear modulus values obtained from tensile testing also decreased in all regions of degenerated samples (Fig. 4-b). This

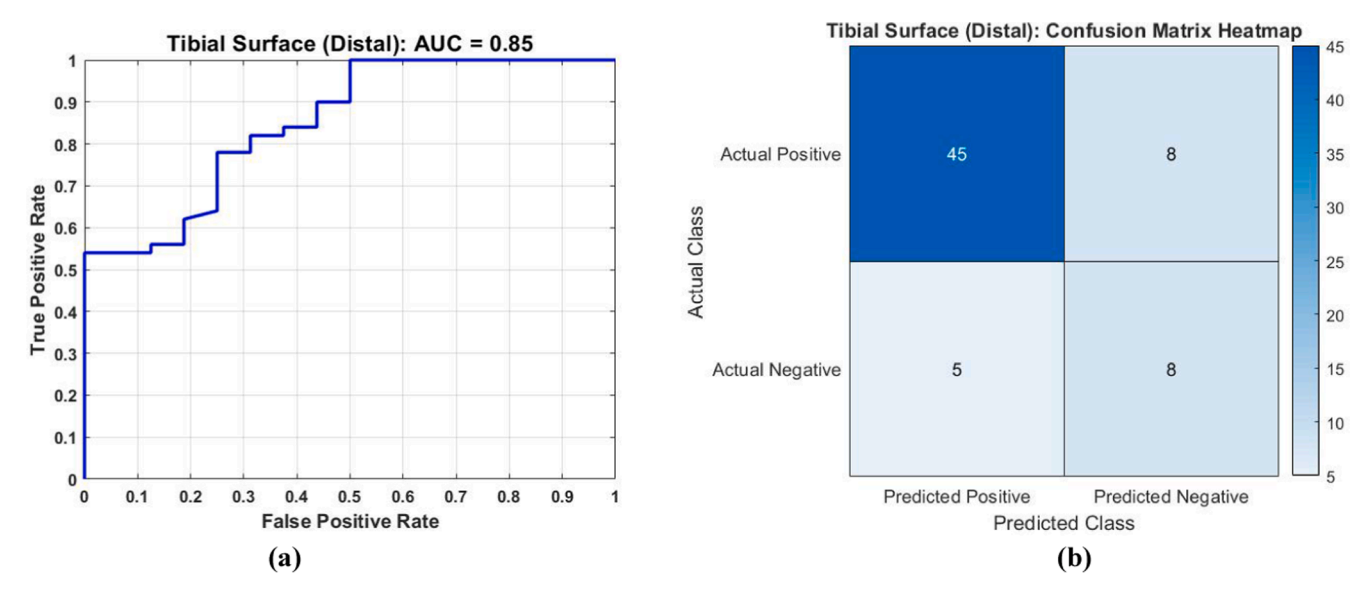


Fig. 9. Tibial layer; a: Receiver operating characteristic curves for ex-vivo shear wave elastography vs. tensile test values, b: Confusion matrix heatmap visually represents the classification results of the diagnostic model.

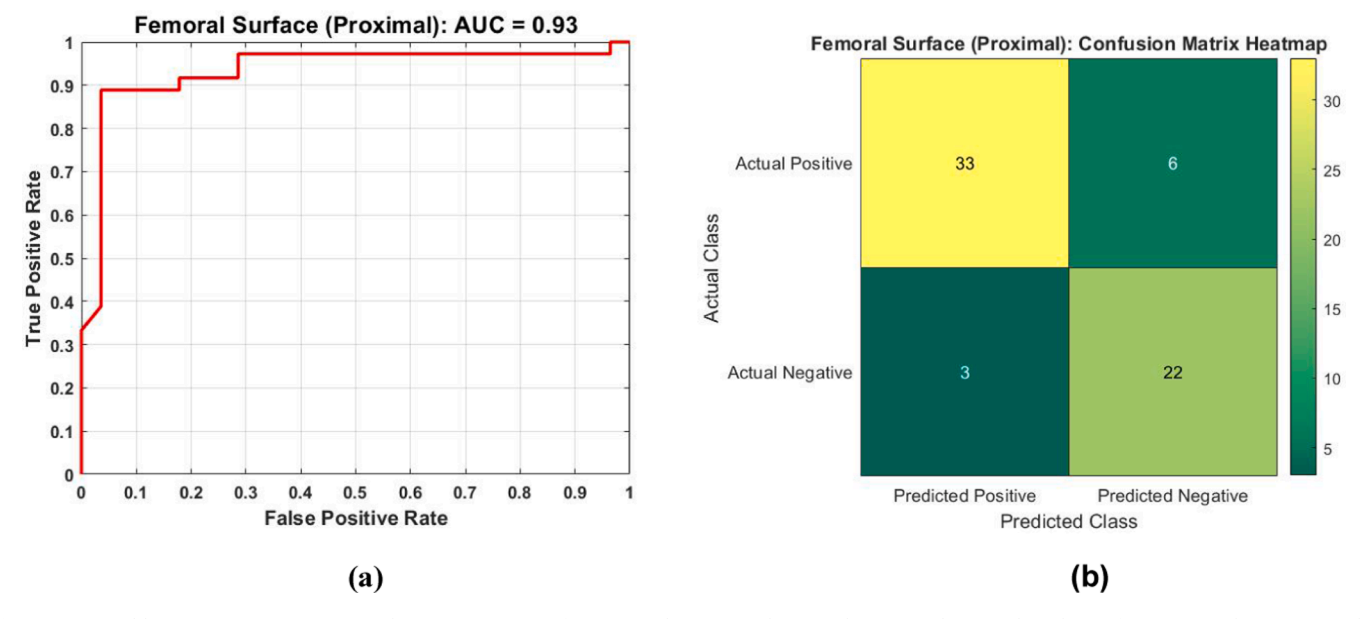


Fig. 10. Femoral layer: a: Receiver operating characteristic curves for ex-vivo shear wave elastography vs. tensile test values, b: Confusion matrix heatmap visually represents the classification results of the diagnostic model.

validation of SSI testing results suggests that it can be a reliable method for assessing the effectiveness of clinical and laboratory tools for evaluating tissue degeneration following freeze treatment. These findings are important because tissue degradation often increases water content, which may weaken shear properties, [6]. This connection is clinically relevant since meniscal degeneration frequently contributes to knee osteoarthritis development and progression, [54]. In frozen menisci, we observed tissue degeneration initiating from the core region, consistent with the histological findings reported by Park et al.[3]. Notably, approximately 50 % of the central area displayed darker discoloration. This observation guided our ROI selection for SSI testing, where we prioritized the deepest accessible tissue depth. Correspondingly, when preparing dumbbell-shaped specimens, we carefully sectioned samples from each region's center toward the tissue curvature extremities.

Our results suggest that, in the context of the meniscus, the linear elasticity theory underlying the SSI method is consistent with the linear

elastic assumption inherent in the biomechanical tensile test.

The correlation between SSI-derived and tensile-test moduli is mechanistically justified through their shared foundation in linear elasticity theory. In SSI, the reconstruction of Young's modulus relies on shear wave propagation physics: the Mach cone formation generates quasi-plane wavefronts whose time-of-flight measurements enable spatial mapping of stiffness[49]. This approach inherently assumes [1] infinitesimal strain (consistent with our tensile-test threshold), [2] isotropic linear elastic behavior at ultrasonic frequencies (despite tissue viscoelasticity, storage modulus dominates in the 50–500 Hz rangeand [3] continuum mechanics validity at the millimeter scale probed by shear wavelengths) [9]. In continuum mechanics, a material body is idealized as being infinitely divisible such that the deformation, stress, and strain are functions of the position of each infinitely small volume within the continuum body[49].

While soft tissues don't support static shear stresses, dynamic shear



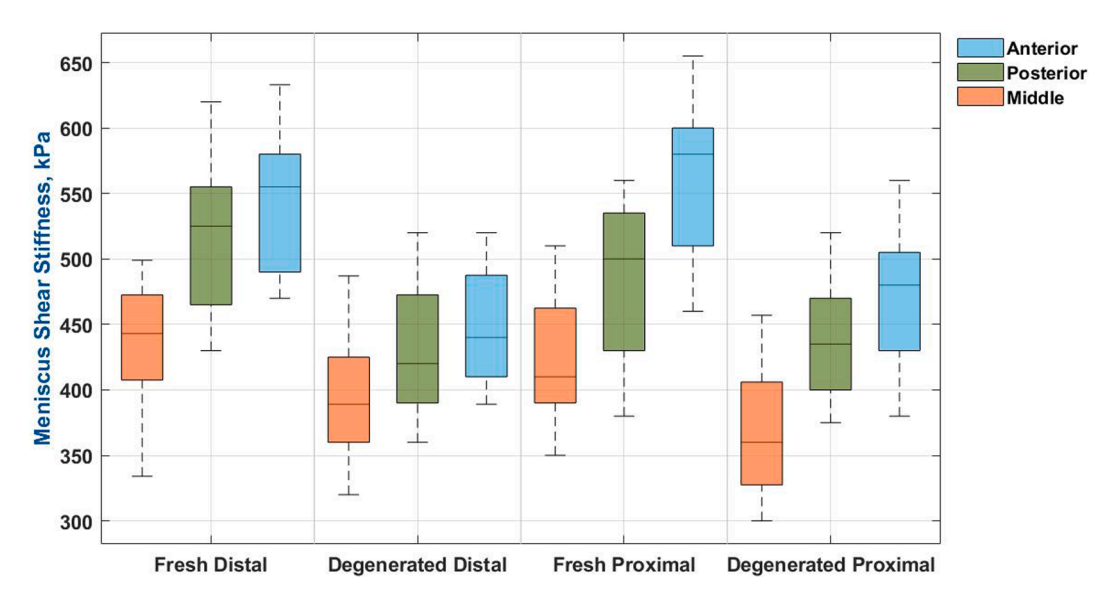


Fig. 11. Comparison of fresh and degenerated menisci sample: SSI Measurements.

wave propagation at ultrasonic frequencies remains governed by the same Hookean relationship ($\mu=\rho c_s^2$) that links shear modulus (μ) to tensile modulus (E) via E $\approx 3\mu$ for nearly incompressible materials ($\nu\approx 0.3$ –0.45) [22,55]. The strong agreement between methods ($r^2=0.81$ –0.94) confirms these assumptions hold for meniscus tissue in the linear regime, with discrepancies in degenerated samples likely arising from structural discontinuities that violate continuum assumptions at larger length scales.

Finaly, SSI uses low-amplitude ARFI excitations (\sim 1–10 µm displacements) with broadband impulses (up to \sim 8 kHz) and repetition frequencies of 100–1000 Hz in short time(ms). At these small strains (<4%), the meniscus behaves as a quasi-elastic solid, dominated by collagen fibrils, with negligible fluid flow and minimal viscous effects. Studies have shown shear modulus variations of less than 5 % across relevant frequencies [22,56], supporting the assumption of frequency-independent shear wave speed. Nonlinear effects, such as collagen fiber recruitment or pyroclastic responses, require much higher deformations (>5% strain or > 50 µm), far exceeding those induced in SSI. Therefore, within the tested range, wave propagation remains in the linear regime, validating the use of constant shear wave velocity for modulus estimation. While biological tissues exhibit viscoelasticity, the assumption of near elasticity [49] is reasonable for the small strains and short time scales (milliseconds) involved in SSI acquisition.

Nevertheless, a notable perspective for future studies is the exploration of nonlinear behaviors exhibited by meniscal tissue and osteoarticular tissue in general, utilizing the SSI methodology. Since Animal models offer significant potential for elucidating the intricate pathophysiology of pain symptoms, their molecular and temporal regulation, and a pivotal pathway for developing and testing symptom-modifying therapeutic interventions[57]. The primary motivation for using both fresh and frozen samples in this study, beyond evaluating the feasibility of SSI and tensile testing in determining reductions in shear modulus, was the limited access of the research community to both healthy and degenerated human samples simultaneously, [34]. This approach allows us to definitively assess the hypothesis that tissue degeneration leads to a reduction in shear and elastic modulus.

4.2. Probe-dependent factor

Significant differences in stiffness measurements between Probes L18-5 and LH20-6 in Supersonic Shear Imaging (SSI) arise from both probe characteristics and preset configurations. In our setup, Probe LH20-6, which has an L-shaped design and a higher central frequency, is

optimized for superficial, high-resolution imaging. In contrast, Probe L18-5, with a conventional linear shape and lower frequency, provides greater depth penetration with reduced resolution. Despite the expectation that higher-frequency probes would generally yield higher stiffness readings in superficial tissues due to increased resolution and sensitivity, our results showed that Probe L18-5 in Meniscus mode consistently produced higher stiffness values than Probe LH20-6 in General mode, while remaining reasonably close to the values recorded with Probe LH20-6 in Knee mode. This apparent contradiction highlights the dominant role of preset selection, beyond just hardware characteristics.

SSI presets (e.g., Meniscus, Knee, General) automatically adjust parameters like push-pulse intensity and detection sensitivity. Meniscus and Knee presets accommodate higher stiffness tissues, enabling broader display ranges and more accurate readings in degenerated zones, unlike the General preset. Additionally, probe frequency impacts shear wave propagation: lower frequencies offer deeper penetration, while higher frequencies provide better resolution but attenuate more rapidly in stiff or deep tissue, [46].

Therefore, even when the same anatomical region is examined, the depth-dependent mechanical heterogeneity of the meniscus and differences in shear wave frequency content result in probe-dependent variability in stiffness readings. We observed that although the absolute values differed significantly between these two modes, they were strongly correlated, confirming that the relative stiffness trends were preserved across presets, (see Fig. 12).

4.3. Technical factors in stiffness measured by SSI

As demonstrated in Fig. 12, Comparison of mean measurements across probescan be attributed to several key technical and methodological factors related to probe characteristics and shear wave elastography configuration. First, excitation frequency and depth penetration play a critical role: high-frequency probes (e.g., 6–9 MHz) offer enhanced resolution for superficial tissues but have limited penetration, while lower-frequency probes (e.g., 2–4 MHz) enable deeper imaging at the cost of resolution. This directly affects shear wave velocity measurements due to the meniscus's depth-dependent mechanical heterogeneity, [9,22,50]. Second, displacement field and focal zone characteristics vary between probes, with each generating unique acoustic radiation force profiles. A narrower focal zone may lead to underestimation of stiffness in deeper or heterogeneous regions, [22,58]. Third, shear wave detection sensitivity is influenced by

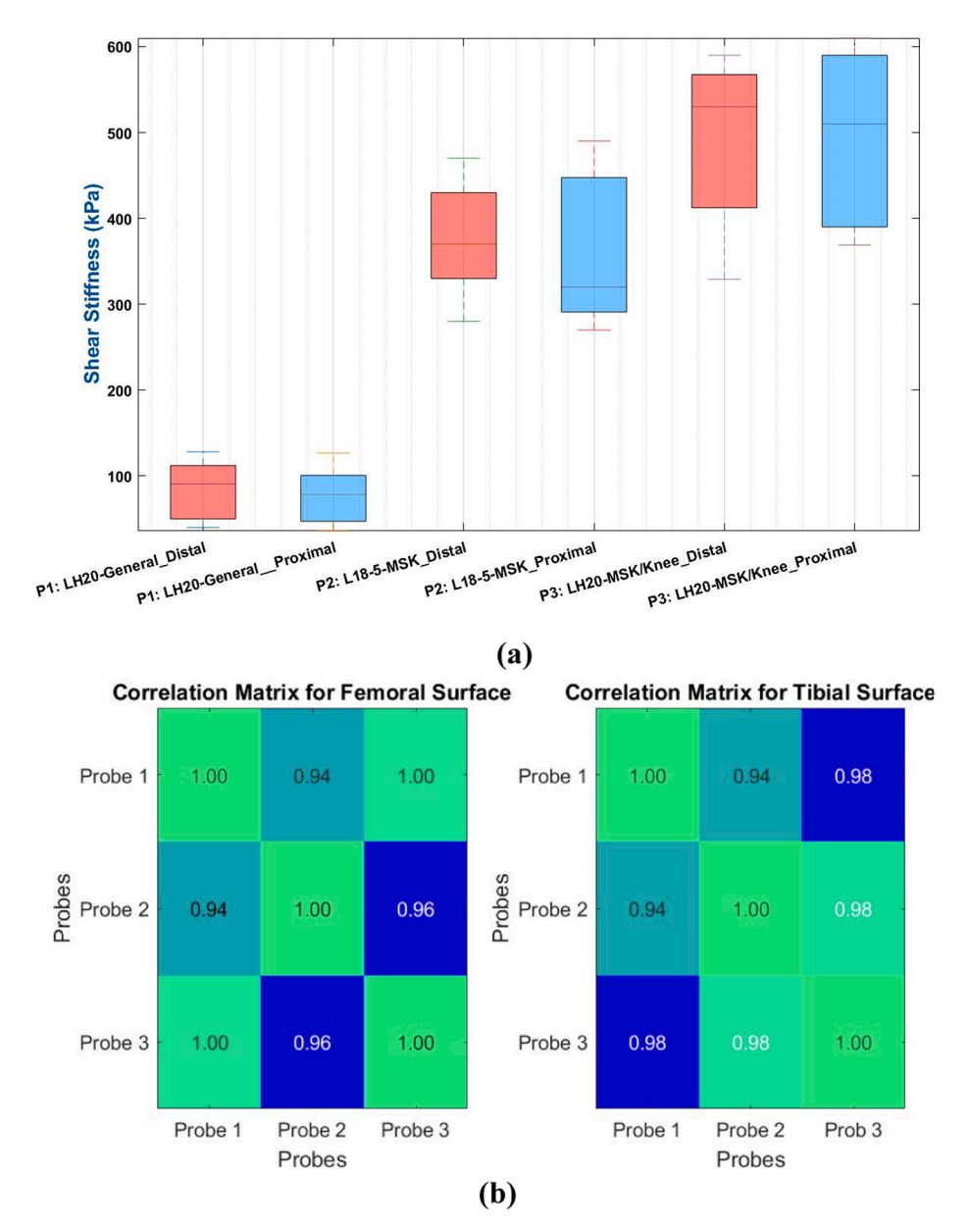


Fig. 12. a: Comparison of mean measurements across probes, b: correlation matrix for femoral and tibial surface, Probes 1, 2 and 3 represent LH20-General, L18-5-MSK/Meniscus and LH20-MSK/Knee, respectively, across Anterior, Central and Posterior Correlation.

differences in tracking beam alignment and Doppler sensitivity, which alter the signal-to-noise ratio, especially in anisotropic tissues such as the meniscus, [55]. Fourth, probe-specific postprocessing algorithms, including manufacturer-dependent time-to-peak or phase-tracking methods, can introduce systematic measurement biases[49]. Despite these absolute differences, the correlation across measurement modes remains strong: stiffer samples consistently appear stiffer across probes, indicating that the underlying biological variation is reliably captured through different acoustic windows. These factors collectively explain the observed discrepancies while reinforcing the internal consistency and reliability of relative stiffness trends across devices.

4.4. ROI-dependent factors on measurements and stiffness metrics

In addition, the selection and diameter of the ROI are found to be of critical importance. This assertion is supported by the findings of a review of previous literature and tensile test results, which indicate that the blue, green, and yellow regions displayed by the SSI system are reproducible, while red and orange regions were avoided. In line with

the findings of studies conducted on organs such as the breast, tendons, liver, and thyroid, it has been demonstrated that ROI diameter can significantly affect elastic parameter values, thereby influencing result accuracy and repeatability, [51]. Our analysis confirmed that selecting a larger ROI size has a more pronounced impact on **Emax** values due to the greater likelihood of including collagen fibers and proteoglycans within the measurement area. Therefore, an optimal ROI size of 3 mm was determined, with the most reproducible SSI-reported parameters being "**Emean**" and "**Emin**" values, showing 91 % and 83 % accuracy, respectively. These selections yielded particularly reliable results for degenerated samples, as meniscal degeneration, as previously mentioned, originates from the central core of the tissue[59].

4.5. Methodological Basis for SWE in meniscal assessment

To assess the validity of supersonic shear wave elastography (SWE) for estimating bovine meniscus shear modulus, key biophysical and methodological factors were evaluated. The meniscus thickness (8–15 mm) relative to shear wavelengths suggests guided wave propagation

rather than bulk waves. While boundary reflections could theoretically occur, geometric attenuation and consistent modulus measurements across ROIs indicate minimal impact. Although 3D wave simulations would provide definitive confirmation, experimental conditions (localized excitation, probe positioning) reduce reflection artifacts. The observed wave behavior can be explained by the presence of guided Lamb wave modes, where low-frequency phase velocities approach the theoretical shear wave speed $(\sqrt{(\mu/\rho)})$, although the guided nature of the waves causes dispersion because of the geometry (still examining the real part of the wave number) even for a Lamb wave. It seems that, as explained in Sections 4-6, the meniscus inhomogeneity generates nonclassical dispersion, potentially involving mode coupling (Ao-So), shear horizontal (SH) waves, and frequency-cutoff effects, the rigorous investigation of which is deferred to future research. This is supported by prior dispersion curve analyses in porcine menisci showing 6-14 m/s velocities in comparable frequency ranges (250-600 Hz), [22]. Geometric attenuation and consistent modulus values across ROIs suggest minimal boundary reflection artifacts. While phase velocity measurements were not performed here, time-of-flight measurements in this frequency band provide a practical estimate of shear modulus, consistent with established SWE protocols for anisotropic tissues.

The significant correlation between SWE-derived moduli and those obtained from quasi-static tensile testing confirms the validity of this approach, despite the assumption of wave dispersion. Since SWE operates in the small-strain regime and at frequencies where the storage modulus dominates over the loss modulus, viscoelastic effects are minimized, and shear modulus remains largely strain-rate independent. Therefore, complex dispersion analysis is unnecessary for the study's objective and would add limited value relative to the primary goal of intrinsic property extraction.

The validity of SWE measurements is further supported by the anatomical alignment between tensile loading and the circumferential collagen fiber orientation in the meniscus, existing literature demonstrating SWE reliability in thin, anisotropic tissues with guided wave propagation, and consistent findings from prior cartilage and tendon studies that have validated stiffness assessment in similar anisotropic environments(21) [55].

Importantly, the ROIs in this study were located within the proximal meniscus (depths of $8-15\,$ mm), corresponding to the central, mechanically homogeneous region characterized by peripheral fiber alignment. Within this range, shear modulus values were statistically consistent with tensile test results.

4.6. Integrated Depth-Dependent SSI results

A depth-dependent variation in shear modulus was observed across 126 regional measurements (63 menisci × 2 posterior regions per meniscus) taken from the outer circumferential band of the tissue. Analysis focused on regions of maximum thickness, predominantly found in the posterior segment. Specifically, when the probe was placed on the proximal surface, shear stiffness initially decreased from 6 to ~ 9 mm depth (p = 0.018, r = -0.68), followed by stabilization and a slight increase toward for 9-16 mm (p = 0.043, r=+0.28). In contrast, a monotonic decrease in stiffness was observed across the same depth range, (6 to 15 mm), when the probe was positioned on the distal surface (p = 0.023, r = -0.59). Quantitatively, SSI measurements in the 6-9 mm depth range showed a stronger correlation with tensile testing (r = 0.904) than in the 9-15 mm range (r = 0.809), indicating higher accuracy in shallower regions, also it has been demonstrated that the superficial meniscal layers exhibit functional homogeneity across the three distinct regions: the anterior, central, and posterior regions [8]. These trends are in agreement with prior phantom-based findings [60], which demonstrated a general decrease in measured shear modulus with increasing depth due to shear wave attenuation and signal-to-noise ratio (SNR) loss.

The non-linear trend seen with proximal-side probe placement may

be attributed to the layered structure of the meniscus. The initial decrease corresponds to wave propagation through the proximal and middle layers—characterized by lower fiber alignment and greater heterogeneity—while the slight increase in the 12–15 mm range likely reflects the transition into the denser, circumferentially aligned distal layer. This transition is anatomically supported by meniscal microstructure literature, [6,8,22] and further reinforced by the higher stiffness values observed at greater depths from the proximal surface compared to the same depths from the distal side. In the proximal alignment, corresponding to the central, deeper layer of the meniscus where collagen fibers are predominantly circumferential, variations in shear stiffness values with depth are consistent with the expected structural organization.

Although direct SNR metrics were not extracted in this study, intra-ROI signal variability was monitored and remained within acceptable limits [22]. Future studies will focus on depth-dependent shear stiffness mapping across different meniscal regions and layers, supported by SNR analysis and histological validation and advanced data analysis. Importantly, ROI depth and probe orientation must be carefully controlled in SSI studies of the meniscus, as these factors significantly influence elastographic accuracy. These findings provide foundational evidence for depth-aware elastography protocols and highlight the need for computational modeling to separate wave modes and correct for depth-induced measurement artifacts in complex, anisotropic tissues like the meniscus.

4.7. Translational Outlook and research perspectives

The clinical translation of these findings is supported by several key considerations. First, SSI shows strong potential for early diagnosis of meniscal degeneration, serving as a valuable complement to existing MRI and ultrasound techniques by detecting mechanical changes prior to visible structural damage, particularly in accessible regions such as the anterior horn and peripheral zones using conventional high-frequency transducers. Second, the method could be adapted for intra-operative applications, where real-time stiffness mapping may guide surgical decisions during arthroscopic meniscal repair or resection procedures. Third, our demonstration of SSI's sensitivity to freeze—thawinduced degeneration in 60 bovine specimens suggests its utility for postoperative monitoring of tissue remodeling following meniscal interventions.

While conducted in an ex vivo model, these results provide the fundamental validation needed for ongoing development of motion-compensated 3D SSI protocols for human applications. The significant correlation between SSI-derived measurements and mechanical testing standards (R2 > 0.9) underscores the technique's potential to transform clinical approaches to meniscal assessment, offering orthopedic practice a reliable, quantitative tool for evaluating tissue integrity without invasive procedures. Future work will focus on adapting these methods for in vivo use through optimized transducer positioning and motion compensation algorithms.

Note that although the results demonstrate acceptable correlation and agreement, differences in measured values must be considered. These discrepancies may stem from assumptions of elasticity and homogeneity, as the meniscus does not fully satisfy these conditions.

This study evaluates two key aspects: firstly, the non-destructive extraction of meniscus stiffness, and secondly, the diagnostic capability of the SSI method. Given the high correlation between the elastography test and linear and nonlinear mechanics, the reliability of the SSI measurements is assured. The same subject, especially from the perspective of pathology and MRI approval for osteoarticular tissue, and secondly, the significant number of samples tested in this research can emphasize the strength of the reliability of SSI measurements.

Overall, the findings of this study indicate that SSI should be applied in studies focused on distinguishing variations between participants or monitoring changes over time. This includes in vivo pathology

detection, assessing the effects of rehabilitation interventions, and exploring meniscal biomechanics and their adaptability (or lack thereof) to external and internal factors. Secondly, due to the predictive validation of stiffness values obtained by SSI for both small (<4% strain) and large strains, this method holds promise as a reliable tool for ex vivo testing and a potential diagnostic approach for in vivo injury detection. Thirdly, the considerable number of measured samples and the comprehensive examination of different regions reinforce the reproducibility and robustness of SSI measurements when compared to the gold standard tensile testing method.

Fourthly, this study confirms the absence of significant measurement differences between operators, the effectiveness of the fixed mechanical arm, and the consistency of results across different musculoskeletal transducers. Additionally, it highlights the importance of precise selection of the region of interest (ROI) in the diagnostic process.

From a biomechanical perspective, a more extensive study is still needed, incorporating a substantial sample size with varying degrees of degeneration for in vitro human samples. Such a study should assess collagen content, water content, equilibrium modulus, permeability parameters, and extract dynamic solid and fluid phase parameters under compression to further evaluate SSI stiffness measurements against solid-phase parameters. This could enhance the biomechanical understanding of SSI measurements for osteoarticular tissues, even though the diagnostic significance of tissue stiffness values derived from SWE elastography has been clearly demonstrated in this study. Furthermore, investigating the potential of SSI for nonlinear stiffness measurements could serve as a foundation for future research in this field.

5. Conclusion

The observations of this study indicate that ultrasound supersonic shear imaging (SSI) measurements are correlated with tissue stiffness, both for small strains in the tibial and femoral regions and for large strains in the peripheral region. The findings demonstrated that SSI possesses the capacity to predict the ultimate stiffness and the corresponding Young's modulus for the circumferential region, as well as the shear modulus resulting from the small strain in the nonlinear stressstrain region for the femoral/tibial region, with 88 % and 90 % accuracy, respectively. Stiffness values obtained from real-time elastography testing were lower across all regions in degenerated samples compared to fresh samples. Similarly, shear modulus values obtained from tensile testing also decreased in all regions of degenerated samples. When utilizing SWE technology to assess the meniscus, it is advisable to position an ROI with a diameter of 2 or 3 mm and use E-mean as the elasticity index, also the consistency of results across different musculoskeletal transducers were confirmed. These findings significantly enhance our understanding of elastography's effectiveness in biomechanical research and its potential applications in diagnosing and managing musculoskeletal disorders. In conclusion, SSI is a validated, accurate, and sensitive technique for assessing meniscal shear modulus, making it a valuable tool for studying meniscus biomechanics and improving orthopedic patient care.

Declaration of competing interest

The authors declare that they have no known competing financial interests or personal relationships that could have appeared to influence the work reported in this paper.

Acknowledgment

This research was funded by grant PID2023-1479010B-I00 funded by MICIU/AEI/10.13039/501100011033 and by ERDF, EU, and Funding for open access charge: Universidad de Granada/CBUA. research was supported by Grant PCI2022-135048-2 funded by MICIU/AEI/ 10.13039/501100011033 and by the European Union Next Generation

EU/PRTR (G.R.), research was supported by Listen2Future funding by Under grant 101096884; Listen2Future is co-funded by the European Union. Views and opinions expressed are however those of the author(s) only and do not necessarily reflect those of the European Union or Key Digital Technologies Joint Undertaking. Neither the European Union nor the granting authority can be held responsible for them. The project is supported by the Key Digital Technologies Joint Undertaking and its members including top-up funding by Austria, Belgium, Czech Republic, Germany, Netherlands, Norway, and Spain. Lastly, research was supported by Consejería de Universidad, Investigación e Innovación from Junta de Andalucía, P21.00182 (G.R.).

Data availability

All the data are available within the main manuscript.

References

- [1] C.M. Gupte, A.M.J. Bull, R.D. Thomas, A.A. Amis, The meniscofemoral ligaments: secondary restraints to the posterior drawer: analysis of anteroposterior and rotary laxity in the intact and posterior-cruciate-deficient knee, The Journal of Bone & Joint Surgery British Volume, 85 (5) (2003) 765–773.
- [2] L. McCann, E. Ingham, Z. Jin, J. Fisher, Influence of the meniscus on friction and degradation of cartilage in the natural knee joint, Osteoarthr. Cartil. 17 (8) (2009) 995–1000.
- [3] J.Y. Park, J.K. Kim, J.E. Cheon, M.C. Lee, H.S. Han, Meniscus stiffness measured with shear wave elastography is correlated with meniscus degeneration, Ultrasound Med. Biol. 46 (2) (2020) 297–304.
- [4] I. McDermott, Meniscal tears, repairs and replacement: their relevance to osteoarthritis of the knee, Br. J. Sports Med. 45 (4) (2011) 292–297.
- [5] Y. Sun, S. Sun, L. Chen, L. Liu, P. Song, W. Li, Y. Yu, L. Fengzhu, J. Qian, H. Wang, Flame retardant and mechanically tough poly (lactic acid) biocomposites via combining ammonia polyphosphate and polyethylene glycol, Compos. Commun. 6 (2017) 1–5.
- [6] E.A. Makris, P. Hadidi, K.A. Athanasiou, The knee meniscus: structure–function, pathophysiology, current repair techniques, and prospects for regeneration, Biomaterials 32 (30) (2011) 7411–7431.
- [7] G. Jacob, K. Shimomura, A.J. Krych, N. Nakamura, The meniscus tear: a review of stem cell therapies, Cells 9 (1) (2019) 92.
- [8] J.T. Moyer, R. Priest, T. Bouman, A.C. Abraham, T.L.H. Donahue, Indentation properties and glycosaminoglycan content of human menisci in the deep zone, Acta Biomater. 9 (5) (2013) 6624–6629.
- [9] J. Bercoff, M. Tanter, M. Fink, Supersonic shear imaging: a new technique for soft tissue elasticity mapping, IEEE Trans. Ultrason. Ferroelectr. Freq. Control 51 (4) (2004) 396–409.
- [10] A. Brazy, E.E.W. Van Houten, Homogenous Shear Modulus Reconstruction at multiple frequencies using the DICE Method, Results Eng. 9 (2021) 100198.
- [11] H. Uehara, Y. Itoigawa, T. Wada, D. Morikawa, A. Koga, Y. Maruyama, M. Ishijima, Shear wave elastography correlates to degeneration and stiffness of the long head of the biceps tendon in patients undergoing tenodesis with arthroscopic shoulder surgery, J. Shoulder Elbow Surg. 33 (1) (2024) e31–e41.
- [12] Z.J. Zhang, S.N. Fu, Shear elastic modulus on patellar tendon captured from supersonic shear imaging: correlation with tangent traction modulus computed from material testing system and test–retest reliability, PLoS One 8 (6) (2013) e68216.
- [13] M. Ali, J. Hoffman, J. Clark, S. Takak, Modeling of impact response of composite graded structure, ASME International Mechanical Engineering Congress and Exposition (2011).
- [14] Y. Wei, K. Alzouhayli, N.D. Schilaty, A.W. Hooke, J.L. Sellon, N.A. Bates, Viability of shear wave elastography to predict mechanical/ultimate failure in the anterolateral and medial collateral ligaments of the knee, J. Biomech. 174 (2024) 112264
- [15] T. Götschi, J. Widmer, F. Cornaz, J. Kimenai, J.M. Spirig, J.G. Snedeker, M. Farshad, Region-and degeneration dependent stiffness distribution in intervertebral discs derived by shear wave elastography, J. Biomech. 121 (2021) 110395.
- [16] P. Corrigan, J.A. Zellers, P. Balascio, K.G. Silbernagel, D.H. Cortes, Quantification of mechanical properties in healthy Achilles tendon using continuous shear wave elastography: a reliability and validation study, Ultrasound Med. Biol. 45 (7) (2019) 1574–1585.
- [17] G. Evripides, C.P. Loizou, P. Christodoulides, Using structural equation modeling and intima-media complex texture features to assess cardiovascular disease risk in the common carotid artery, Results Eng. 24 (2024) 103613.
- [18] E. Gurun, I. Akdulum, M. Akyuz, N. Tokgoz, S.O. Oktar, Shear wave elastography evaluation of meniscus degeneration with magnetic resonance imaging correlation, Acad. Radiol. 28 (10) (2021) 1383–1388.
- [19] E.A. Gonzalez-Leon, J.C. Hu, K.A. Athanasiou, Yucatan minipig knee meniscus regional biomechanics and biochemical structure support its suitability as a large animal model for translational research, Front. Bioeng. Biotechnol. 10 (2022) 844416.

- [20] H. Palnitkar, R. Reiter, S. Majumdar, J. Crutison, S. Lin, T.J. Royston, D. Klatt, 1-Norm waveform analysis for MR elastography-based quantification of inhomogeneity: Effects of the freeze-thaw cycle and Alzheimer's disease, J. Mech. Behav. Biomed. Mater. 157 (2024) 106636.
- [21] J. Sun, L. Westover, K. Wu, L. Laouar, N.M. Jomha, S. Adeeb, G.M. Thornton, Tensile mechanical properties of vitrified porcine menisci are superior to frozen and similar to fresh porcine menisci, J. Biomech. 143 (2022) 111277.
- [22] S.S. Hashemi, A. Callejas, A. Valera, A. Ruiz Molina, J.L. Martin-Rodriguez, G. Rus, Feasibility of ultrasound elastography for meniscus viscoelastic Assessment: Ex vivo porcine validation and pilot human study, Mater. Des. 256 (2025) 114197.
- [23] Spivak AE, Demin IY. Description and implementation of the Supersonic Shear Imaging method on the Verasonics research system. Journal of Physics: Conference Series; 2020: IOP Publishing.
- [24] H. Latorre-Ossa, J.L. Gennisson, E. De Brosses, M. Tanter, Quantitative imaging of nonlinear shear modulus by combining static elastography and shear wave elastography, IEEE Trans. Ultrason. Ferroelectr. Freq. Control 59 (4) (2012) 833–839.
- [25] E. Hohmann, N. Keough, V. Glatt, K. Tetsworth, R. Putz, A. Imhoff, The mechanical properties of fresh versus fresh/frozen and preserved (Thiel and Formalin) long head of biceps tendons: a cadaveric investigation, Annals of Anatomy-Anatomischer Anzeiger. 221 (2019) 186–191.
- [26] Y. Deng, N.C. Rouze, M.L. Palmeri, K.R. Nightingale, Ultrasonic shear wave elasticity imaging sequencing and data processing using a verasonics research scanner, IEEE Trans. Ultrason. Ferroelectr. Freq. Control 64 (1) (2016) 164–176.
- [27] S. Hashemi, S.A. Galehdari, Numerical and experimental study of energy absorption of PLA calibrated honeycomb structures under quasi-static loading, J. Braz. Soc. Mech. Sci. Eng. 46 (1) (2024) 26.
- [28] M. Kucewicz, P. Baranowski, J. Malachowski, A method of failure modeling for 3D printed cellular structures, Mater. Des. 174 (2019) 107802.
- [29] S.S. Hashemi, H. Hatami, Z. Ahmad, Impact loading response and plasticity stress flow analysis of multilayer low carbon steel: a study of mechanical properties and deformation characteristics, Case Stud. Constr. Mater. (2025) e04721.
- [30] T. Long, K. Vemaganti, J.E. Hawes, C.Y. Lin, An experimental study of the heterogeneity and anisotropy of porcine meniscal ultimate tensile strength, J. Mech. Behav. Biomed. Mater. 157 (2024) 106649.
- [31] A. Morejon, P.L. Dalbo, T.M. Best, A.R. Jackson, F. Travascio, Tensile energy dissipation and mechanical properties of the knee meniscus: relationship with fiber orientation, tissue layer, and water content, Front. Bioeng. Biotechnol. 11 (2023) 1205512.
- [32] X.Y. Yin, J.Y. Chung, D.Y. Park, H.K. Song, B.K. Kim, H.W. Bae, K.H. Park, B. H. Min, The perimensical capsule: potential supporting structure surrounding meniscus, Cartilage 13(1_suppl):208S-15S (2021).
- [33] D.Q. Nesbitt, D.N. Siegel, N. Danielle, S.J. Nelson, T.J. Lujan, Effect of age on the failure properties of human meniscus: High-speed strain mapping of tissue tears, J. Biomech. 115 (2021) 110126.
- [34] D. Warnecke, J. Balko, J. Haas, R. Bieger, F. Leucht, N. Wolf, N.B. Schild, S.E. C. Stein, A.M. Seitz, A. Ignatius, Degeneration alters the biomechanical properties and structural composition of lateral human menisci, Osteoarthr. Cartil. 28 (11) (2020) 1482–1491.
- [35] B.PE. An, Investigative Study Toward the Development of a Crosslinked Porcine Xenograft Meniscus Total Replacement, Mississippi State University, 2017.
- [36] J.M. Peloquin, M.H. Santare, D.M. Elliott, Advances in quantification of meniscus tensile mechanics including nonlinearity, yield, and failure, J. Biomech. Eng. 138 (2) (2016) 021002.
- [37] R. Mitchell, R. Pitts, Y.M. Kim, M.J. Matava, Medial meniscal root avulsion: a biomechanical comparison of 4 different repair constructs, Arthroscopy: the Journal of Arthroscopic & Related Surgery. 32 (1) (2016) 111–119.
- [38] S.H. Yan, H.K. Ou-Yang, Y.L. Shan, D.Z. Luo, H. Wang, K. Zhang, Tensile biomechanical characteristics of human meniscus, Emerging Mater. Res. 5 (1) (2015) 44-49
- [39] E.H. Lakes, C.L. Kline, P.S. McFetridge, K.D. Allen, Comparing the mechanical properties of the porcine knee meniscus when hydrated in saline versus synovial fluid, J. Biomech. 48 (16) (2015) 4333–4338.

- [40] K.M. Fischenich, J. Lewis, K.A. Kindsfater, T.S. Bailey, T.L. Haut Donahue, Effects of degeneration on the compressive and tensile properties of human meniscus, J. Biomech. 48 (2015) 1407–1411.
- [41] A. Abdelgaied, M. Stanley, M. Galfe, H. Berry, E. Ingham, J. Fisher, Comparison of the biomechanical tensile and compressive properties of decellularised and natural porcine meniscus, J. Biomech. 48 (8) (2015) 1389–1396.
- [42] M.L. Tanaka, N. Vest, C.M. Ferguson, P. Gatenholm, Comparison of biomechanical properties of native menisci and bacterial cellulose implant, Int. J. Polym. Mater. Polym. Biomater. 63 (17) (2014) 891–897.
- [43] M. Tissakht, A.M. Ahmed, Tensile stress-strain characteristics of the human meniscal material, J. Biomech. 28 (4) (1995) 411–422.
- [44] D.L. Skaggs, W.H. Warden, V.C. Mow, Radial tie fibers influence the tensile properties of the bovine medial meniscus, J. Orthop. Res. 12 (2) (1994) 176–185.
- [45] D.R. Anderson, D.H. Gershuni, M. Nakhostine, L.A. Danzig, The effects of non-weight-bearing and limited motion on the tensile properties of the meniscus, Arthroscopy: the Journal of Arthroscopic & Related Surgery. 9 (4) (1993) 440–445.
- [46] H. Guerini, X. Ayral, V. Vuillemin, G. Morvan, F. Thévenin, R. Campagna, J. L. Drapé, Ultrasound-guided injection in osteoarticular pathologies: general principles and precautions, Diagn. Interv. Imaging 93 (9) (2012) 674–679.
- [47] T. Mifsud, P. Chatzistergos, C. Maganaris, N. Chockalingam, N. Padhiar, K. M. Stafrace, A. Gatt, Supersonic shear wave elastography of human tendons is associated with in vivo tendon stiffness over small strains, J. Biomech. 152 (2023) 111558.
- [48] X. Cheng, M. Zhang, B. Xu, B. Adhikari, J. Sun, The principles of ultrasound and its application in freezing related processes of food materials: a review, Ultrason. Sonochem. 27 (2015) 576–585.
- [49] J.L. Gennisson, T. Deffieux, M. Fink, M. Tanter, Ultrasound elastography: principles and techniques, Diagn. Interv. Imaging 94 (5) (2013) 487–495.
- [50] C. Ewertsen, J.F. Carlsen, I.R. Christiansen, J.A. Jensen, M.B. Nielsen, Evaluation of healthy muscle tissue by strain and shear wave elastography—Dependency on depth and ROI position in relation to underlying bone, Ultrasonics 71 (2016) 127–133.
- [51] J.H. Lee, S.M. Lee, J.H. Yoon, M.J. Kim, H.I. Ha, S.J. Park, E.S. Kim, K. Lee, J. M. Lee, Impact of respiratory motion on liver stiffness measurements according to different shear wave elastography techniques and region of interest methods: a phantom study, Ultrasonography 40 (1) (2020) 103.
- [52] S. Ahmad, V.A. Singh, A.I. Hussein, Cryopreservation versus fresh frozen meniscal allograft: a biomechanical comparative analysis, J. Orthop. Surg. 25 (3) (2017) 2309499017727946.
- [53] P.B. Lewis, J.M. Williams, N. Hallab, A. Virdi, A. Yanke, B.J. Cole, Multiple freezethaw cycled meniscal allograft tissue: a biomechanical, biochemical, and histologic analysis, J. Orthop. Res. 26 (1) (2008) 49–55.
- [54] M. Englund, A. Guermazi, S.L. Lohmander, The role of the meniscus in knee osteoarthritis: a cause or consequence? Radiologic Clinics. 47 (4) (2009) 703–712.
- [55] J.L. Gennisson, T. Deffieux, E. Macé, G. Montaldo, M. Fink, M. Tanter, Viscoelastic and anisotropic mechanical properties of in vivo muscle tissue assessed by supersonic shear imaging, Ultrasound Med. Biol. 36 (5) (2010) 789–801.
- [56] A.B. Wang, E.J. Perreault, T.J. Royston, S.S.M. Lee, Changes in shear wave propagation within skeletal muscle during active and passive force generation, J. Biomech. 94 (2019) 115–122.
- [57] A.M. Malfait, C.B. Little, J.J. McDougall, A commentary on modelling osteoarthritis pain in small animals, Osteoarthr. Cartil. 21 (9) (2013) 1316–1326.
- [58] J.R. Doherty, G.E. Trahey, K.R. Nightingale, M.L. Palmeri, Acoustic radiation force elasticity imaging in diagnostic ultrasound, IEEE Trans. Ultrason. Ferroelectr. Freq. Control 60 (4) (2013) 685–701.
- [59] C. Pauli, S.P. Grogan, S. Patil, S. Otsuki, A. Hasegawa, J. Koziol, M.K. Lotz, D. D. D'Lima, Macroscopic and histopathologic analysis of human knee menisci in aging and osteoarthritis, Osteoarthr. Cartil. 19 (9) (2011) 1132–1141.
- [60] A. Obrist, L. Ruby, A. Martin, T. Frauenfelder, M. Rominger, C. Paverd, Influence of measurement depth and acquisition parameters on shear wave speed and shear wave dispersion in certified phantoms using a Canon Aplio clinical ultrasound scanner, Ultrasound Med. Biol. 49 (8) (2023) 1742–1759.